Gallouzi, I.E., Parker, F., Chebli, K., Maurier, F., Labourier, E., Barlat, I., Capony, J.P., Tocque, B. & Tazi, J. (1998) A novel phosphorylation-dependent RNase activity of GAP-SH3 binding protein: a potential link between signal transduction and RNA stability. *Mol. Cell. Biol.* **18**, 3956–3965.

Ghisolfi, L., Dutt, S., McConkey, M.E., Ebert, B.L. & Anderson, P. (2012) Stress granules contribute to α-globin homeostasis in differentiating erythroid cells. *Biochem. Biophys. Res. Commun.* **420**, 768–774.

Holley, M.S., Kedersha, N., Dower, K., Rubins, K.H., Anderson, P., Hensley, L.E. & Connor, J.H. (2011) Formation of antiviral cytoplasmic granules during orthopoxvirus infection. *J. Virol.* **85**, 1581–1593.

Irvine, K., Stirling, R., Hume, D. & Kennedy, D. (2004) Rasputin, more promiscuous than ever: a review of G3BP. *Int. J. Dev. Biol.* **48**, 1065–1077.

Kedersha, N. & Anderson, P. (2002) Stress granules: sites of mRNA triage that regulate mRNA stability and translatability. *Biochem. Soc. Trans.* **30**, 963–969.

Kedersha, N., Cho, M.R., Li, W., Yacono, P.W., Chen, S., Gilks, N., Golan, D.E. & Anderson, P. (2000) Dynamic shuttling of TIA-1 accompanies the recruitment of mRNA to mammalian stress granules. *J. Cell Biol.* **151**, 1257–1268.

Kedersha, N.L., Gupta, M., Li, W., Miller, I. & Anderson, P. (1999) RNA-binding proteins TIA-1 and TIAR link the phosphorylation of eIF-2 alpha to the assembly of mammalian stress granules. *J. Cell Biol.* **147**, 1431–1442.

Kennedy, D., French, J., Guitard, E., Ru, K., Tocque, B. & Mattick, J. (2001) Characterization of G3BPs: tissue specific expression, chromosomal localisation and *ras*GAP^{120} binding studies. *J. Cell. Biochem.* **84**, 173–187.

Kim, W.J., Back, S.H., Kim, V., Ryu, I. & Jang, S.K. (2005) Sequestration of TRAF2 into stress granules interrupts tumor necrosis factor signaling under stress condition. *Mol. Cell. Biol.* **25**, 2450–2462.

Kimball, S.R., Horetsky, R.L., Ron, D., Jefferson, L.S. & Harding, H.P. (2003) Mammalian stress granules represent sites of accumulation of stalled translation initiation complexes. *Am. J. Physiol. Cell Physiol.* **284**, 273–284.

Kobayashi, T., Winslow, S., Sunesson, L., Hellman, U. & Larsson, C. (2012) PKCα binds G3BP2 and regulates stress granule formation following cellular stress. *PLoS ONE* **7**, e35820. Doi: 10.1371/journal.pone.0035820.

Soncini, C., Berdo, I. & Draetta, G. (2001) Ras-GAP SH3 domain binding protein (G3BP) is a modulator of USP10, a novel human ubiquitin specific protease. *Oncogene* **20**, 3869–3879.

Sowa, M.E., Bennett, E.J., Gygi, S.P. & Harper, J.W. (2009) Defining the human deubiquitinating enzyme interaction landscape. *Cell* **138**, 389–403.

Stohr, N., Lederer, M., Reinke, C., Meyer, S., Hatzfeld, M., Singer, R.H. & Huttelmaier, S. (2006) ZBP1 regulates mRNA stability during cellular stress. *J. Cell Biol.* **175**, 527–534.

Tourriere, H., Chebli, K., Zekri, L., Courselaud, B., Blanchard, J.M., Bertrand, E. & Tazi, J. (2003) The RasGAP-associated endoribonuclease G3BP assembles stress granules. *J. Cell Biol.* **160**, 823–831.

Tourriere, H., Gallouzi, I.E., Chebli, K., Capony, J.P., Mouaikel, J., Geer, P.V. & Tazi, J. (2001) RasGAP-associated endoribonuclease G3BP: selective RNA degradation and phosphorylation-dependent localization. *Mol. Cell. Biol.* **21**, 7747–7760.

White, J.P., Cardenas, A.M., Marissen, W.E. & Lloyd, R.E. (2007) Inhibition of cytoplasmic mRNA stress granule formation by a viral proteinase. *Cell Host Microbe* **2**, 295–305.

Received: 22 June 2012
Accepted: 7 November 2012

nature COMMUNICATIONS

ARTICLE

Received 18 Apr 2012 | Accepted 15 Aug 2012 | Published 18 Sep 2012

DOI: 10.1038/ncomms2068

p47 negatively regulates IKK activation by inducing the lysosomal degradation of polyubiquitinated NEMO

Yuri Shibata[1], Masaaki Oyama[2], Hiroko Kozuka-Hata[2], Xiao Han[1], Yuetsu Tanaka[3], Jin Gohda[1] & Jun-ichiro Inoue[1,2]

The persistent or excess activation of NF-κB causes various inflammatory and autoimmune diseases, but the molecular mechanisms that negatively regulate NF-κB activation are not fully understood. Here we show that p47, an essential factor for Golgi membrane fusion, associates with the NEMO subunit of the IκB kinase (IKK) complex upon TNF-α or IL-1 stimulation, and inhibits IKK activation. p47 binds to Lys63-linked and linear polyubiquitin chains, which are conjugated to NEMO upon such stimulation. The binding of p47 to polyubiquitinated NEMO triggers the lysosomal degradation of NEMO, thereby inhibiting IKK activation. The silencing of p47 results in enhanced TNF-α- or IL-1-induced IKK activation, and an increased expression of genes encoding inflammatory mediators. Taken together, our results suggest that p47 is critical for negatively regulating stimulation-induced IKK activation in a manner that is mechanistically distinct from the previously characterized negative regulators, such as A20 and CYLD.

[1] Department of Cancer Biology, Division of Cellular and Molecular Biology, Institute of Medical Science, University of Tokyo, Shirokane-dai, Minato-ku, Tokyo 108-8639, Japan. [2] Medical Proteomics Laboratory, Institute of Medical Science, University of Tokyo, Shirokane-dai, Minato-ku, Tokyo 108-8639, Japan. [3] Division of Immunology, Faculty of Medicine, University of the Ryukyus, Nishihara, Okinawa 903-0213, Japan. Correspondence and requests for materials should be addressed to J-i.I. (email: jun-i@ims.u-tokyo.ac.jp).

The post-translational modification of proteins is crucial for the regulation of various intracellular signal transduction pathways. Recent studies have clearly demonstrated that in addition to phosphorylation, ubiquitination is a strategy for regulating biologically important pathways such as those that activate transcription factor nuclear factor-κB (NF-κB)[1–3]. NF-κB is a dimeric transcription factor formed by the Rel/NF-κB family members, including p50, p52, RelA, RelB and c-Rel, and it has crucial roles in immune responses, inflammation, cell proliferation and survival[4]. NF-κB is sequestered in the cytoplasm via its association with inhibitory proteins of the κB family (IκBs) or NF-κB precursors, such as p100 and p105, the C termini of which contain IκB-like ankyrin repeats. The classical NF-κB pathways are activated by cytokines, such as tumour necrosis factor (TNF)-α and interleukin (IL)-1, and bacterial products. Stimulation with these ligands leads to the activation of the IκB kinase (IKK) complex, which consists of the catalytic subunits IKKα and IKKβ, and the regulatory subunit NF-κB essential modulator (NEMO). IKK then phosphorylates IκBs and targets them for Lys48-linked polyubiquitination, which leads to the degradation of ubiquitinated IκBs by the proteasome, allowing NF-κB to enter the nucleus and activate target genes[3]. Alternatively, the non-classical pathways, which are activated by stimulation from CD40, receptor activator of NF-κB or lymphotoxin-β receptor, involve the proteasome-dependent selective degradation of the C-terminal ankyrin repeats of p100 (ref. 5).

In the IL–1R pathway, IKK activation requires the generation of unanchored Lys63-linked polyubiquitin chains[6] or their conjugation to TNF receptor-associated factor (TRAF)-6 (ref. 7) and transforming growth factor-β-activated kinase (TAK)-1 (ref. 8), both of which are catalysed by TRAF6 (E3) and the Ubc13/Uev1A complex (E2)[9]. These Lys63-linked polyubiquitin chains do not induce proteasomal degradation but act as platforms for the formation of active signal complexes that consist of MEKK3, TAK1, TAK1-binding (TAB) 2/TAB3 and the IKK complex, because TAB2/3 and NEMO bind to Lys63-linked polyubiquitin chains via their ubiquitin-binding domains[8,10,11]. This complex formation leads to the activation of TAK1, which then phosphorylates and activates IKKβ[9,12]. Upon TNF-α stimulation, TNF receptor-1 recruits the adaptor TRADD, the E3 ubiquitin ligases TRAF2 and cIAPs, and the kinase RIP1, which results in the polyubiquitination of RIP1 (refs 13–15). The polyubiquitin chain of RIP1 also acts as a platform for the formation of an active TAK1-containing complex. In addition to TAK1 activation, IKK activation requires the stimulation-induced conjugation of Lys63-linked or linear polyubiquitin chains to NEMO[2,16–19], which may induce oligomer formation or a conformational change in NEMO to activate the IKK complex[1]. The former conjugation is catalysed by TRAF6 and the latter by the linear ubiquitin chain assembly complex, which is composed of HOIL-1, HOIP and Sharpin[20–22].

Given that the persistent or excess activation of NF-κB promotes chronic inflammation, autoimmunity and malignancy[23–26], IKK activation needs to be tightly regulated, which highlights the physiological significance of IKK-negative regulators. Among these regulators, two deubiquitinases (DUBs), CYLD and A20, disassemble Lys63-linked or linear polyubiquitin chains, thereby negatively regulating IKK[27–30]. As these two proteins act through distinct molecular mechanisms, they function non-redundantly and their inactivation leads to serious disorders[25,31]. Thus, the polyubiquitin-chain-targeted negative regulation of IKK is crucial for homeostasis.

In the present study, we identified p47 (also known as NSFL1C)[32], a major adaptor of the cytosolic ATPase associated with various cellular activities p97 (ref. 33), as a negative regulator of NF-κB activation. The p47/p97 complex is required for the reassembly of Golgi stacks at the end of mitosis[32–35]. Interestingly, p47 binds to NEMO upon TNF-α or IL-1 stimulation, and induces the lysosome-dependent degradation of polyubiquitinated NEMO without p97, thereby inhibiting IKK activation. Thus, we propose that p47 is involved in a previously unidentified mechanism for the polyubiquitin-chain-mediated negative regulation of NF-κB.

Results

The identification of p47 as a NEMO-binding protein. To identify novel IKK regulators, we searched for proteins that bind to or dissociate from the IKK complex in a manner that is dependent on the Tax protein of the human T-cell leukaemia virus-1. The IKK complex was immunoprecipitated using an anti-Flag antibody from the cytosolic fraction of Jurkat cells that stably expressed Flag-NEMO following the addition of recombinant Tax to activate IKK[36], and the proteins were analysed by mass spectrometry. Among the proteins identified, we focused on p47, because it binds to ubiquitinated proteins via its N-terminal ubiquitin-associated (UBA) domain[37–39] and is involved in the degradation of ubiquitinated proteins[40,41]. Moreover, we found that p47 is exclusively localized in the cytoplasm in various cell lines (Supplementary Fig. S1), although p47 was previously reported to primarily localize to the nucleus in interphase and this was required for its inactivation[42]. A co-immunoprecipitation assay in HEK293T cells that transiently expressed HA–IKKα, IKKβ, or NEMO together with Flag-p47 revealed that NEMO bound to p47, whereas IKKα and IKKβ did not (Fig. 1a). To confirm the interactions under physiological conditions, we co-immunoprecipitated the endogenous proteins in HeLa cells. NEMO-bound p47 appeared after 5 min of stimulation with TNF-α (Fig. 1b) or IL-1 (Fig. 1c). These results indicate that p47 binds to the IKK complex through NEMO in a stimulation-dependent manner.

p47 inhibits TNF-α- or IL-1-induced IKK activation. To understand whether p47 affects IKK activation, we first examined the effect of p47 overexpression using *in vitro* kinase assays. TNF-α-induced IKK activation was significantly reduced by p47 overexpression (Fig. 1d), whereas p47 knockdown resulted in enhanced TNF-α-induced IKK activation (Fig. 1e). Moreover, p47 knockdown increased the phosphorylation and degradation of IκBα (Fig. 1f,g). The enhanced phosphorylation of IκBα by p47 knockdown was observed 5 min after TNF-α or IL-1 stimulation, consistent with the kinetics of the stimulation-induced association of p47 with NEMO (Fig. 1b,c). Although p47 is reported to be involved in various fundamental processes associated with cell division[32–35], p47 knockdown had no effect on proliferation, survival or endoplasmic reticulum (ER) stress (Supplementary Fig. S2), which strongly suggests that the enhanced NF-κB activation following p47 knockdown is not due to non-specific effects. Taken together, these results indicate that p47 negatively regulates TNF-α- and IL-1-induced IKK activation. p47 also inhibits Tax-induced IKK activation (Supplementary Fig. S3). In addition, p47 knockdown slightly enhanced the TNF-α- and IL-1-induced activation of JNK and p38, but not that of ERK (Fig. 1f,g), which is consistent with the previous finding that NEMO is necessary for full JNK and p38 activation[43]. The lack of a significant effect of p47 knockdown on the level of phosphorylated p38 in non-stimulated cells suggests that cell stress is barely induced by p47 knockdown (Fig. 1f,g).

p47 negatively regulates NF-κB-driven transcription. To understand whether p47 affects the NF-κB-mediated transcription, we first checked the nuclear DNA-binding activity of NF-κB with an electrophoretic mobility shift assay. Nuclear NF-κB was significantly enhanced in p47-knockdown cells upon TNF-α and IL-1 stimulation (Fig. 2a). To measure the transcriptional activity of NF-κB, HEK293T cells were transfected with the NF-κB reporter plasmid, and the subsequent TNF-α stimulation- or p65 overexpression-induced luciferase activity was measured. p47 inhibited TNF-α-induced NF-κB activation in a dose-dependent manner but

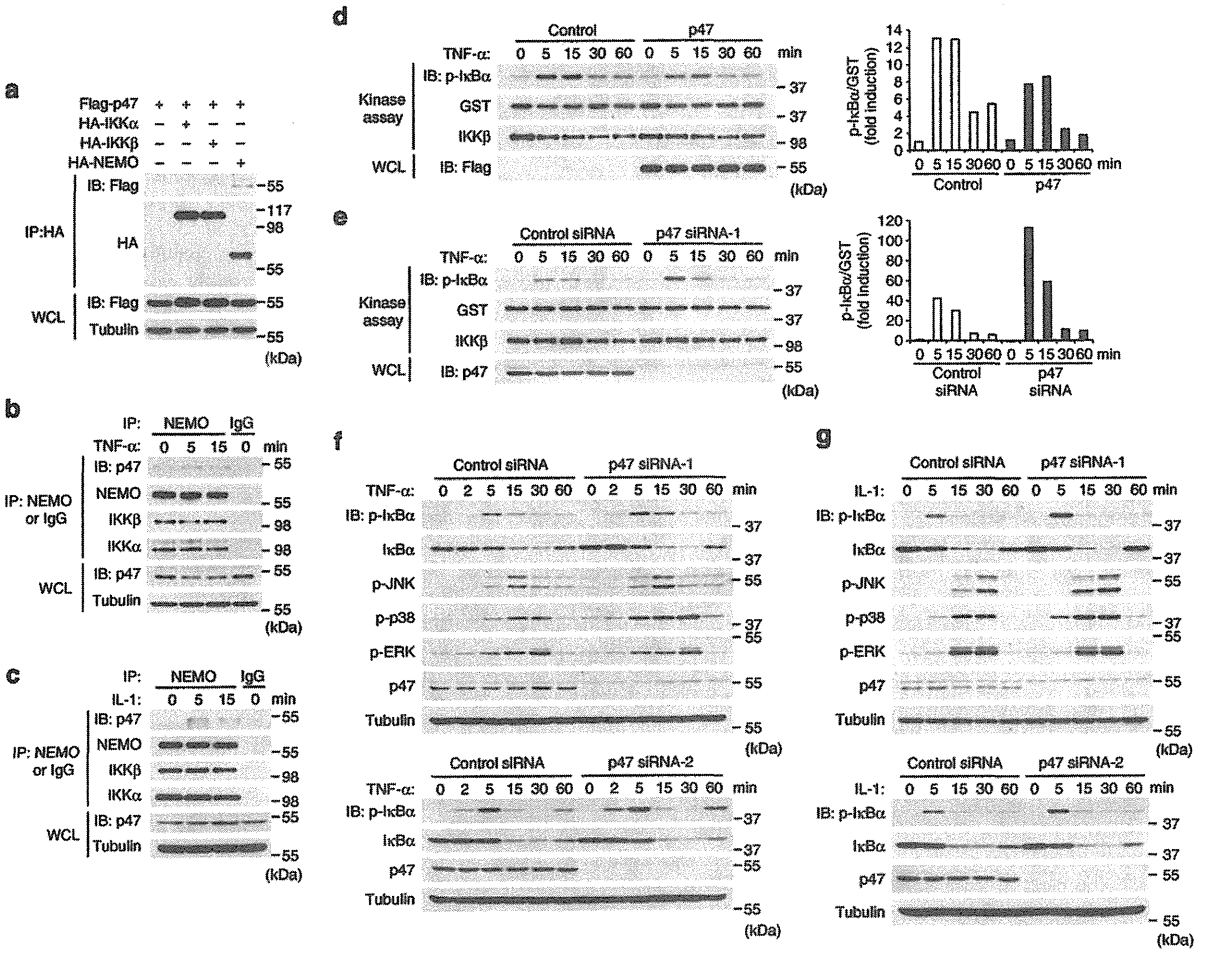

Figure 1 | The identification of p47 as a negative regulator of TNF-α- and IL-1-induced IKK activation. (**a**) HEK293T cells were transfected with a Flag-p47 expression plasmid (0.3 μg) together with a plasmid encoding HA-IKKα, HA-IKKβ or HA-NEMO (4 μg). Cell lysates were subjected to immunoprecipitation with an anti-HA antibody followed by immunoblotting with anti-HA and anti-Flag antibodies. Whole-cell lysate (WCL) was also prepared and analysed by immunoblotting with anti-Flag and anti-tubulin antibodies. (**b**,**c**) HeLa cells were treated with TNF-α (10 ng ml^{-1}, **b**) or IL-1 (10 ng ml^{-1}, **c**). Cell lysates were subjected to immunoprecipitation with a control IgG or anti-NEMO antibody followed by immunoblotting with the indicated antibodies. The WCL was analysed by immunoblotting with anti-p47 and anti-tubulin antibodies. (**d**) HEK293T cells were transfected with a control or a Flag-p47 expression plasmid. After 48 h, the cells were treated with TNF-α (10 ng ml^{-1}). The IKK complex that had been immunoprecipitated with an anti-NEMO antibody was incubated at 30 °C for 1 h in a reaction mixture containing recombinant GST-IκBα (amino acids 1–54) followed by immunoblotting with anti-p-IκBα, anti-GST and anti-IKKβ antibodies. The relative activities of the IKK complex are expressed as the intensity of the band detected by the anti-p-IκBα antibody divided by the intensity detected by the anti-GST antibody. The intensities of the bands were quantified using ImageJ software (National Institutes of Health). (**e**) HEK293T cells were transfected with control or p47 siRNA-1. After 72 h, the cells were treated with TNF-α (10 ng ml^{-1}). The IKK kinase assay was performed as described in **d**. (**f**,**g**) HeLa cells were transfected with control, p47 siRNA-1 or p47 siRNA-2. After 72 h, the cells were treated with TNF-α (1 ng ml^{-1}, **f**) or IL-1 (3 ng ml^{-1}, **g**). The WCL was analysed by immunoblotting with the indicated antibodies. The depicted results are representative of three independent experiments.

had no effect on p65-mediated transcription (Fig. 2b,c), indicating that p47 targets the IKK complex but has no effect on events that are downstream of IKK activation, such as the nuclear translocation or phosphorylation-mediated activation of p65 (ref. 44). As p47 knockdown resulted in a significant enhancement in TNF-α-induced NF-κB activity (Fig. 2d), we investigated the physiological significance of the p47-mediated negative regulation of NF-κB by measuring the expression levels of the NF-κB target genes. The TNF-α- or IL-1-induced expression of *Il8* and *Tnfa* was notably enhanced in p47-knockdown cells (Fig. 2e), indicating that the p47-mediated negative regulation of IKK activation significantly affects NF-κB-driven transcription.

p47 regulates IKK in a CYLD- and A20-independent manner. We then addressed whether CYLD or A20 is involved in p47-mediated inhibition of IKK activation. The expression levels of CYLD and A20 were not affected by p47 knockdown at all time points tested (Fig. 3a,b), and p47 knockdown enhanced the phosphorylation of IκBα in *Cyld*- or *A20*-deficient mouse embryonic fibroblast (MEF) cells (Fig. 3c–f). These results indicate that p47 inhibits IKK activation in an A20- and CYLD-independent manner.

Ubiquitin-binding of p47 is crucial for IKK inhibition. To elucidate the molecular mechanisms of p47-mediated IKK inhibition, we sought to determine the structural requirements for the inhibitory

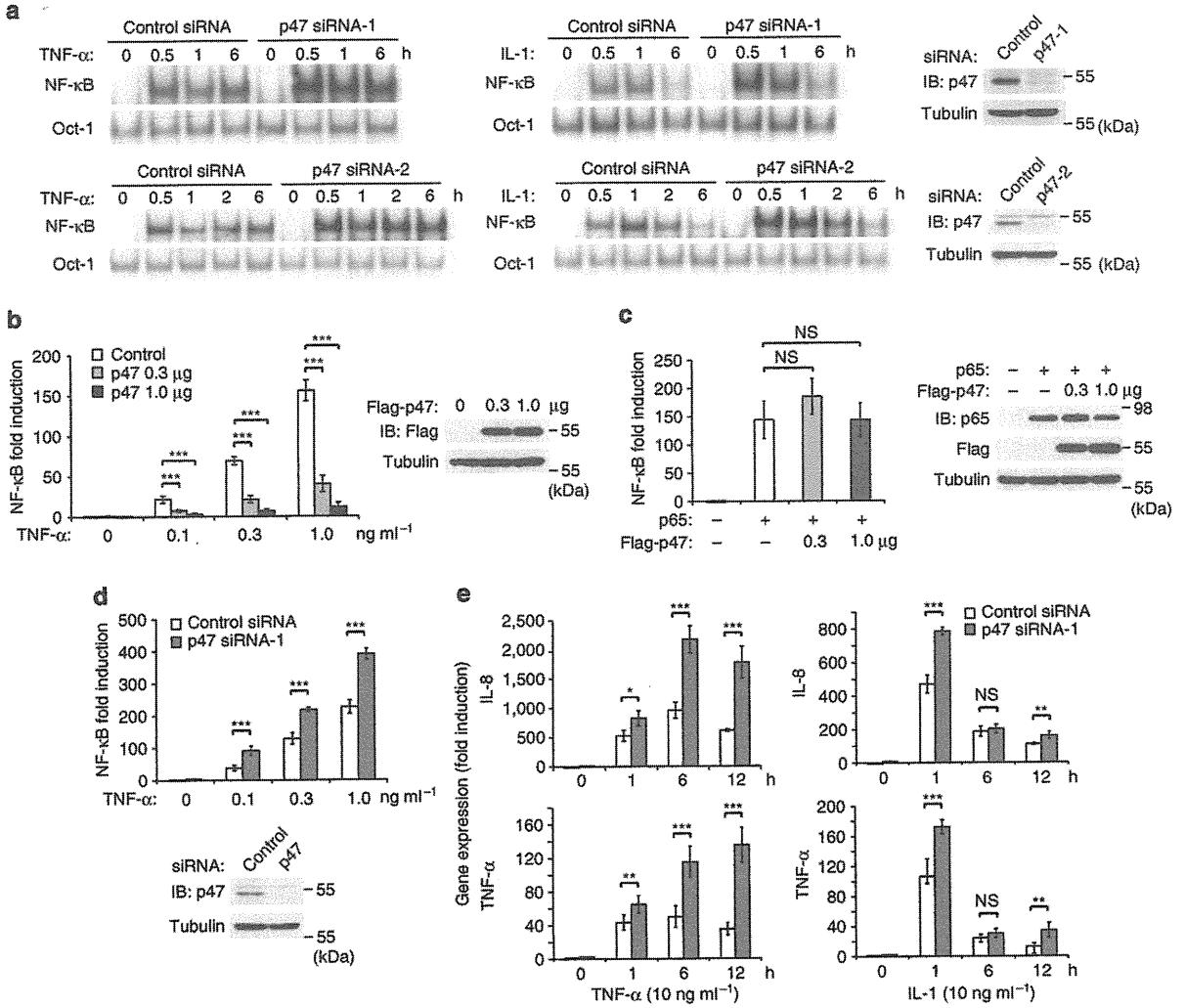

Figure 2 | p47 negatively regulates NF-κB-driven transcription. (**a**) HeLa cells that had been transfected with control, p47 siRNA-1 or p47 siRNA-2 were treated with TNF-α (10 ng ml^{-1}) or IL-1 (10 ng ml^{-1}). Nuclear extracts were subjected to electrophoretic mobility shift assay. The efficiency of p47 knockdown is shown. The depicted results are representative of three independent experiments. (**b**) HEK293T cells were transfected with a 3×κB-luc reporter and a Flag-p47 expression plasmid. The cells were treated with TNF-α for 24 h, and the resultant luciferase activity was measured. The fold induction was calculated by dividing each luciferase activity by that of the control without TNF-α stimulation. (**c**) HEK293T cells were transfected with a 3×κB-luc reporter and a p65 expression plasmid in combination with increasing amounts of a Flag-p47 expression plasmid. After 48 h, the subsequent luciferase activity was measured. The fold induction was calculated by dividing each luciferase activity by that of the control without p65 expression. (**d**) HEK293T cells were transfected with control or p47 siRNA-1. The cells were then transfected with a 3×κB-luc reporter and treated with TNF-α for 24 h, and the subsequent luciferase activity was measured. Fold induction was calculated by dividing each luciferase activity by that of the control siRNA treatment without TNF-α stimulation. (**e**) HeLa cells were transfected with control or p47 siRNA-1. After 60 h, the cells were treated with TNF-α or IL-1. The expression levels of IL-8 and TNF-α were measured by real-time RT–PCR. The fold induction was calculated by dividing each expression value by that of a control siRNA treatment without TNF-α or IL-1 stimulation. The results shown in **b**, **c**, **d** and **e** indicate the mean±s.d. ($n=3$). NS, not significant. Statistical significance was assessed using a Student's *t*-test. ***$P<0.01$, **$P<0.02$ and *$P<0.05$.

effect of p47 on IKK. p47 consists of three known domains: the N-terminal UBA domain (1–45)[45], the central SEP (shp1, eyc and p47) domain (179–246)[39] and the C-terminal ubiquitin regulatory X (UBX) domain (286–370)[46] (Fig. 4a). p47 is crucial for the p97-mediated membrane fusion events that occur during the reassembly of the ER, the nuclear envelope and the Golgi apparatus[32–35]. As the ubiquitin-binding activity of p47 (via its UBA domain) and the association of p47 with p97 are essential for the p97-mediated reassembly of these organelles[32,37], we first investigated whether similar conditions are required for p47-mediated IKK inhibition. To properly analyse the abilities of various p47 mutants to inhibit endogenous IKK, we silenced endogenous p47 before introducing expression vectors for p47 mutants, because p47 forms a trimer[32,39]. We constructed small interfering RNA (siRNA)-resistant p47 and the following p47 deletion mutants: ΔUBA (46–370) lacking the UBA domain, ΔUBX (1–246) lacking essential regions for p97 binding[47], and ΔUBA/SEP (247–370) lacking the UBA and SEP domains and the linker sequence between them (Fig. 4a). The p47-knockdown cells were transfected with expression vectors encoding p47-WT or deletion mutants together with the NF-κB reporter. Both p47-WT

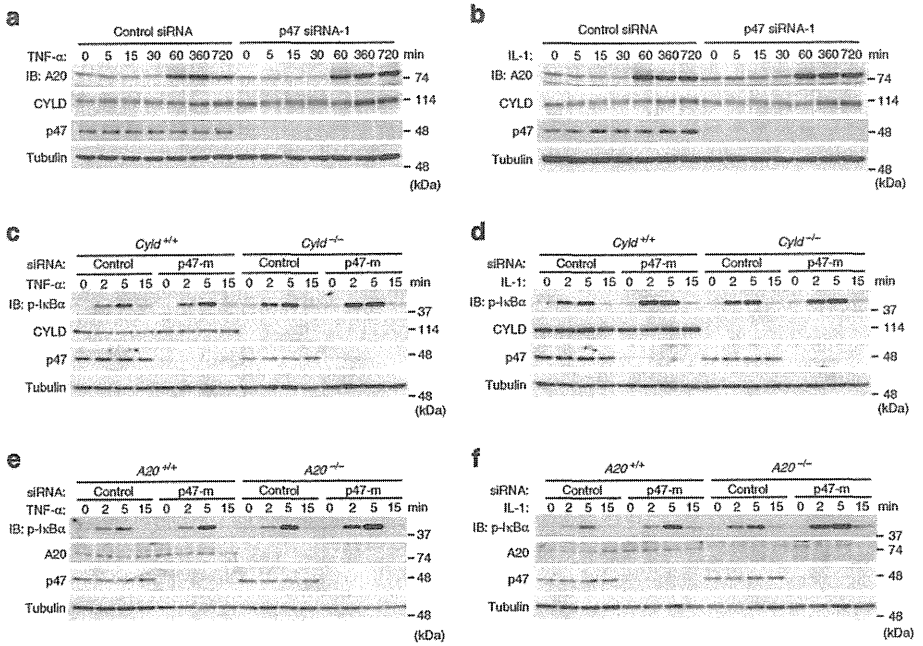

Figure 3 | p47 negatively regulates TNF-α- and IL-1-induced IKK activation independently of CYLD and A20. (**a**,**b**) HeLa cells were transfected with control or p47 siRNA-1. After 60 h, the cells were treated with TNF-α (10 ng ml^{-1}, **a**) or IL-1 (10 ng ml^{-1}, **b**) for the indicated times. The whole-cell lysate (WCL) was analysed by immunoblotting with the indicated antibodies. (**c**,**d**) *Cyld*$^{+/+}$ or *Cyld*$^{-/-}$ MEFs were transfected with control or p47 siRNA-mouse. After 72 h, the cells were treated with TNF-α (3.0 ng ml^{-1}, **c**) or IL-1 (3.0 ng ml^{-1}, **d**) for the indicated times. The WCL was analysed by immunoblotting with the indicated antibodies. (**e**,**f**) *A20*$^{+/+}$ or *A20*$^{-/-}$ MEFs were transfected with control or p47 siRNA-mouse. After 72 h, the cells were treated with TNF-α (3.0 ng ml^{-1}, **e**) or IL-1 (3.0 ng ml^{-1}, **f**) for the indicated times. The WCL was analysed by immunoblotting with the indicated antibodies. p47-m, p47-mouse. The depicted results are representative of three independent experiments.

and ΔUBX blocked NF-κB activation equally well (Fig. 4b), suggesting that the association of p47 with p97 is not essential for IKK inhibition. ΔUBA had a significantly reduced ability to inhibit NF-κB activation (Fig. 4b), indicating that the ubiquitin-binding activity of p47 is crucial for IKK inhibition. Interestingly, ΔUBA/SEP almost completely lacked the inhibitory effect (Fig. 4b), revealing that the sequence containing the SEP domain and linker region is also involved in IKK inhibition, albeit to a lesser extent than the UBA domain. To confirm the dispensability of p97, we examined the effect of p97 knockdown on the p47-mediated inhibition of NF-κB-driven reporter activity. p97 knockdown was successful because p97 was not detected, and the spliced form of *XBP1* mRNA, an indication of ER stress, was observed[48] (Fig. 4c). p97 knockdown barely affected the p47-mediated inhibition of NF-κB-driven reporter activity (Fig. 4c), indicating that p97 is dispensable for the p47-mediated inhibition of NF-κB activation. Consistent with the results shown in Figure 4b, p47-WT and ΔUBX bound similarly to NEMO, whereas the interaction of ΔUBA or ΔUBA/SEP with NEMO was barely observed (Fig. 4d). To further address the requirement for the ubiquitin-binding activity, we generated the V15A/L34A/Y42A mutant, wherein the three amino acid residues in the UBA domain that have been shown to form tight contacts with ubiquitin were substituted with alanines[39,49] (Fig. 4a). The V15A/L34A/Y42A mutant exhibited significantly reduced NEMO-binding activity (Fig. 4d). Taken together, both the p47/NEMO interaction and p47-mediated IKK inhibition require the ubiquitin-binding, but not the p97-binding activity of p47.

p47 binds to Lys63-linked and linear polyubiquitin chains. NEMO becomes conjugated with either Lys63-linked or linear polyubiquitin chains upon stimulation[1,16–19]. Thus, we next determined which types of polyubiquitin linkages are recognized by p47. Purified recombinant wild-type or mutant His_6-p47 protein bound to Ni-NTA resin (Fig. 5a) was mixed with various recombinant polyubiquitin chains, which were composed of di-ubiquitin and higher molecular weight species up to hepta-ubiquitin. p47 similarly bound to Lys48-linked tetra-ubiquitin, Lys63-linked tetra-ubiquitin, and linear tri- and tetra-ubiquitins (Fig. 5b). However, for polyubiquitin chains longer than tetra-ubiquitin, p47 preferentially bound to Lys63-linked and linear polyubiquitin chains than Lys48-linked polyubiquitin chains (Fig. 5b). Given that a large proportion of polyubiquitin chains in mammalian cells are likely to be longer than tetra-ubiquitin, these results suggest that p47 preferentially binds to Lys63-linked and linear polyubiquitin chains rather than Lys48-linked polyubiquitin chains *in vivo*. The UBA domain is primarily involved in binding to all three types of polyubiquitin chains (Fig. 5c–e). The region composed of the SEP domain and linker region is also involved in binding to both Lys63-linked and linear polyubiquitin chains, although to a much lesser extent than the UBA domain (Fig. 5c,d).

To confirm that the binding of p47 to NEMO is mediated by the polyubiquitin chains conjugated to NEMO, recombinant His_6-NEMO was incubated with His_6-UBE1 (E1), His_6-Ubc13/Uev1 (E2), His_6-TRAF6 (E3) and ATP to catalyse the Lys63-linked polyubiquitination of NEMO. As a control experiment, the same reaction was carried out without ATP. The immunocomplexes precipitated by an anti-NEMO antibody were incubated with recombinant wild-type or mutant p47 and subjected to immunoblotting. As the extent of NEMO ubiquitination was similar in the reactions with ATP and as comparable amounts of NEMO and other proteins (except p47) co-precipitated in all of the reactions (Fig. 5f), wild-type or mutant p47 bound to NEMO could be measured by immunoblotting, using

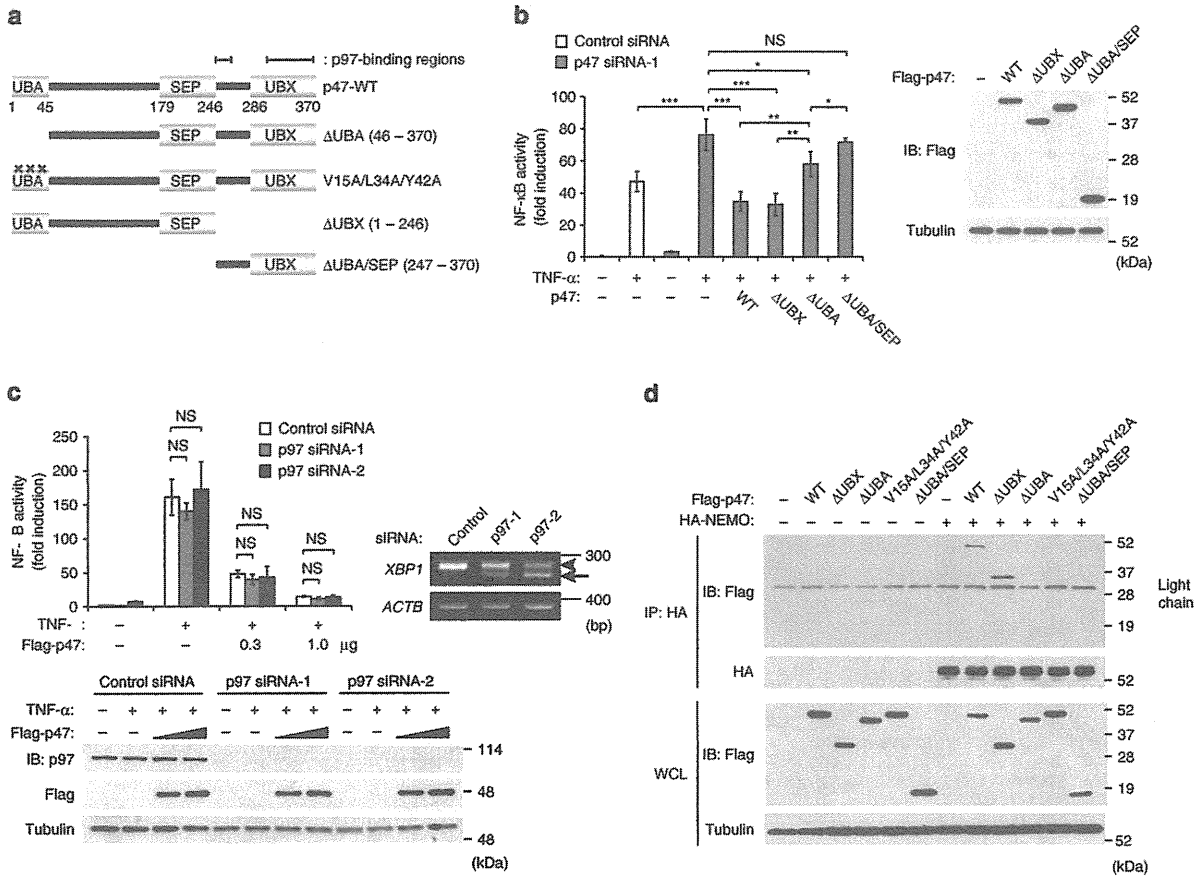

Figure 4 | The ubiquitin-binding activity of p47 is crucial for p47-mediated IKK inhibition. (**a**) A schematic representation of various mutants of p47. (**b**) HEK293T cells were transfected with control or p47 siRNA-1. After 24 h, the cells were transfected with plasmids encoding Flag-p47 or its various mutants together with a 3×κB-luc reporter. After 24 h, the cells were treated with TNF-α (1.0 ng ml^{-1}) for 24 h, and the subsequent luciferase activity was measured. The results are given as the mean±s.d. (n=3). NS, not significant. Statistical significance was assessed using a Student's t-test. ***P<0.01, **P<0.02 and *, P<0.05. The expression levels of p47 and its various mutants were analysed. (**c**) HEK293T cells were transfected with control, p97 siRNA-1 or p97 siRNA-2. After 24 h, the cells were transfected with a 3×κB-luc reporter and Flag-p47 expression plasmid (0.3 or 1.0 μg). The cells were then treated with TNF-α (1.0 ng ml^{-1}) for 24 h, and the subsequent luciferase activity was measured. The fold induction was calculated by dividing each luciferase activity measurement by that of the cells transfected with control siRNA without TNF-α stimulation. The results are given as the mean±s.d. (n=3). NS, not significant. Immunoblotting was performed using the WCL to confirm the silencing of p97 and expression levels of p47. RT-PCR was performed to detect unspliced (arrow head) and spliced (arrow) *XBP1* mRNA to confirm that the silencing of p97 induced ER stress. (**d**) HEK293T cells were transfected with expression plasmids encoding Flag-p47 or its various mutants (0.3 μg) together with a HA-NEMO expression plasmid (4 μg). After 24 h, the cell lysates were prepared and subjected to immunoprecipitation with an anti-HA antibody followed by immunoblotting with anti-Flag and anti-HA antibodies. The WCL was analysed by immunoblotting with anti-Flag and anti-tubulin antibodies. The depicted results are representative of three independent experiments.

the anti-p47 antibody. p47 was observed to bind to NEMO only when NEMO was conjugated to Lys63-linked polyubiquitin chains, and this interaction required the ubiquitin-binding activity of p47 (Fig. 5f). To further confirm the linkage-type specificity, recombinant His_6-NEMO was subjected to *in vitro* ubiquitination using cIAP1 as an E3 enzyme, with ubiquitin containing only Lys-48 or only Lys-63 to generate NEMO with Lys48-linked or Lys63-linked polyubiquitin chains[14,50]. p47 bound to NEMO with Lys63-linked polyubiquitin chains, but not to NEMO with Lys48-linked chains (Fig. 5g). Moreover, p47 failed to bind to NEMO in the presence of CYLD (Fig. 5h). Taken together, these results indicate that p47 does not bind to the non-ubiquitinated form of NEMO, but does bind to NEMO conjugated with Lys63-linked or linear polyubiquitin chains.

p47 post-translationally controls NEMO protein levels . Given that p47 binds to polyubiquitinated NEMO, we hypothesized that p47 may induce the degradation of polyubiquitinated NEMO, because p47 is involved in the degradation of polyubiquitinated proteins[38]. Each of the components of the IKK complex, including IKKα, IKKβ, NEMO and Hsp90, was expressed in HEK293T cells with or without p47. Whereas the expression levels of IKKα, IKKβ and Hsp90 were not affected (Fig. 6a), NEMO expression was decreased by co-expression of p47 in a dose-dependent manner (Fig. 6b). As the promoters that drive NEMO and Hsp90 expression were the same, the reduction in NEMO expression could not be due to transcriptional squelching. p47 knockdown resulted in enhanced HA-NEMO expression derived from the transfected plasmid, whereas complementation with Flag-p47 resulted in decreased

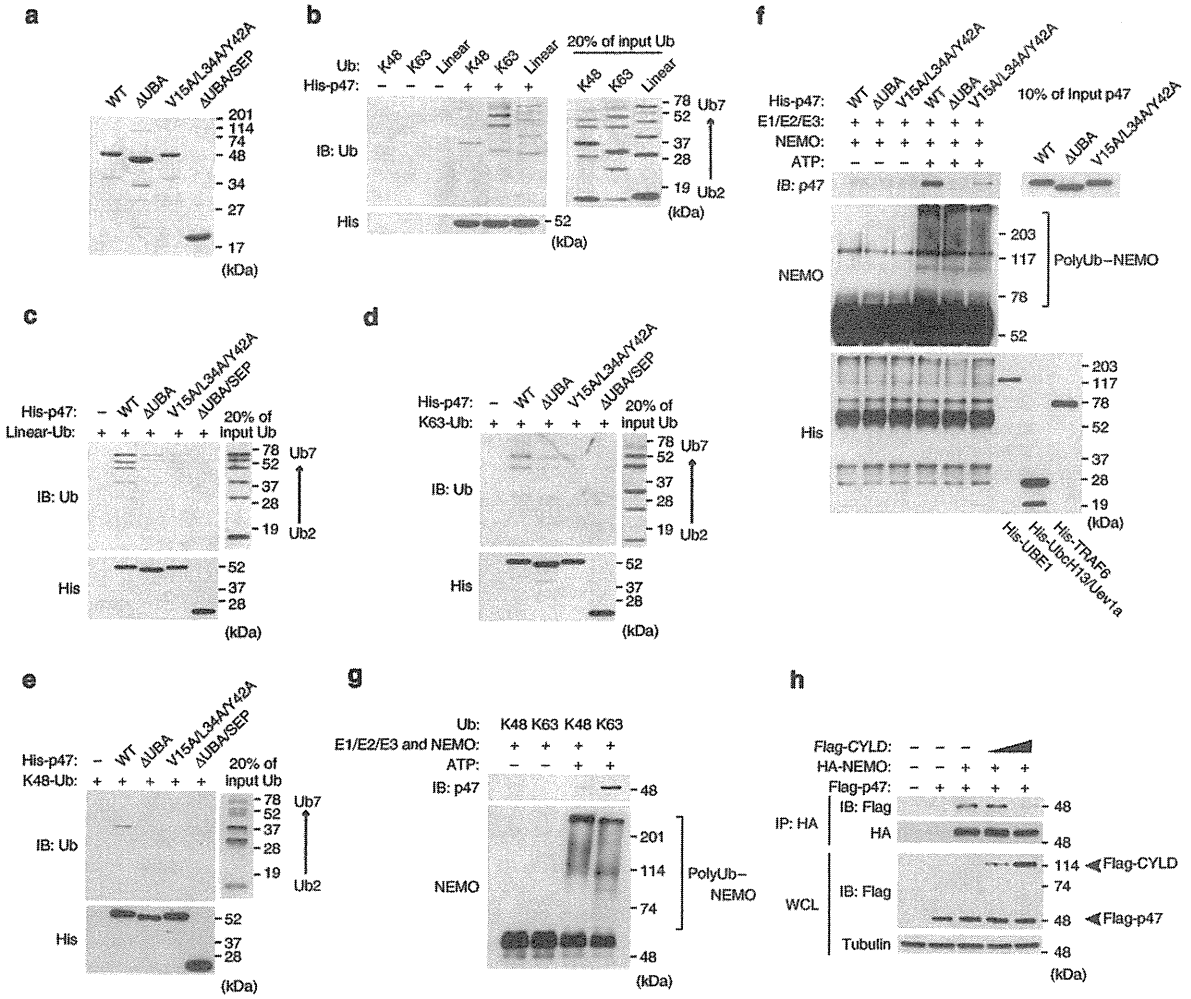

Figure 5 | The UBA domain of p47 preferentially interacts with Lys-63-linked and linear polyubiquitin chains. (**a**) The analysis of recombinant p47 and its mutant with 10% SDS–PAGE. (**b**) Ni-NTA resin-bound recombinant p47 or control resin was incubated with Lys48-linked, Lys63-linked, or linear polyubiquitin chains (Ub_{2-7}). Polyubiquitin chains bound to p47 and a 20% input of polyubiquitin chains were analysed by immunoblotting with an anti-Ub antibody. (**c**–**e**) Recombinant p47 and various mutants that were bound to Ni-NTA resin were incubated with linear (**c**), Lys63-linked (**d**) or Lys48-linked polyubiquitin chains (**e**). (**f**) Recombinant His_6-NEMO was incubated with recombinant His_6-UBE1 (E1), His_6-UbcH13/Uev1a (E2), His_6-TRAF6 (E3) and ubiquitin in the presence or the absence of ATP. The reaction mixtures were then incubated with anti-NEMO antibody and protein G-sepharose. The immunoprecipitates were incubated with recombinant His_6-p47 or its mutants, washed and analysed by immunoblotting with anti-p47, anti-NEMO and anti-His_6 antibodies. Ten percent of the inputs of p47 and its mutants were analysed by immunoblotting with an anti-p47 antibody. (**g**) Recombinant His_6-NEMO was incubated with UBE1 (E1), UbcH5c (E2), His_6-cIAP1 (E3), and ubiquitin containing only lysine 48 (K48) or only lysine 63 (K63) in the presence or the absence of ATP. The reaction mixtures were incubated with an anti-NEMO antibody and protein G-sepharose. The immunoprecipitates were incubated with recombinant His_6-p47, washed and analysed by immunoblotting with anti-p47 and anti-NEMO antibodies. (**h**) HEK293T cells were transfected with expression plasmids encoding HA-NEMO (1.0 μg) and Flag-p47 (0.3 μg) in combination with the expression plasmid for Flag-CYLD (0.3, 3.0 μg). After 48 h, the cell lysates were subjected to immunoprecipitation with an anti-HA antibody followed by immunoblotting with anti-Flag and anti-HA antibodies. The WCL was analysed by immunoblotting with anti-Flag and anti-tubulin antibodies. The depicted results are representative of three independent experiments.

HA-NEMO expression (Fig. 6c). The expression level of HA-IKKβ derived from the co-transfected plasmid was not affected by p47 knockdown or subsequent complementation thereof (Fig. 6c). As NEMO is an integral component of the IKK complex, we next addressed whether p47 degrades IKKβ-associated NEMO. HEK293T cells were co-transfected with expression plasmids for NEMO, HA-IKKβ and Flag-p47. Immunoprecipitation of IKKβ revealed that p47 degraded IKKβ-associated NEMO (Fig. 6d). NEMO expression, but not IKKβ expression, was significantly reduced even when they were co-expressed (Fig. 6d). In addition, the overexpression of p47 resulted in a reduction of endogenous NEMO after, but not before, TNF-α stimulation, although the extent of the endogenous NEMO reduction was less significant than that of overexpressed NEMO (Fig. 6e). These results strongly suggest that p47 selectively degrades NEMO and leaves IKKα/β intact upon stimulation. p97 knockdown barely affected the p47-mediated reduction of NEMO (Fig. 6f). The ubiquitin-binding activity of p47 was crucial for the p47-mediated reduction of NEMO,

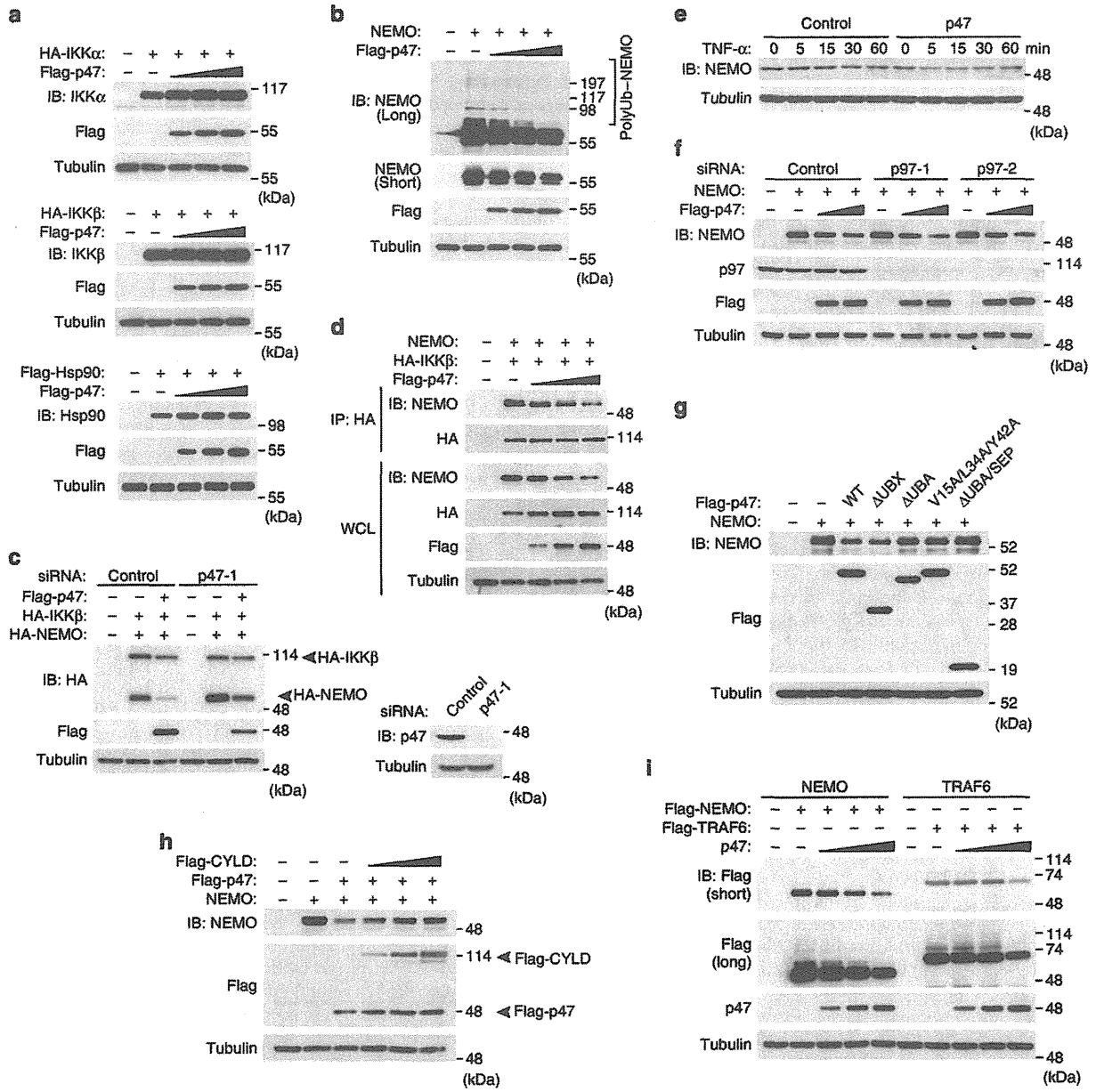

Figure 6 | p47 reduces NEMO protein expression. (**a**) HEK293T cells were transfected with an HA-IKKα, HA-IKKβ, or Flag-Hsp90 expression plasmid (0.1 μg) together with a Flag-p47 expression plasmid (0.1, 0.3 or 1 μg). (**b**) HEK293T cells were transfected with a NEMO expression plasmid (0.1 μg) together with a Flag-p47 expression plasmid (0.1, 0.3 or 1 μg). (**c**) HEK293T cells were transfected with control or p47 siRNA. After 24 h, the cells were transfected with a control or Flag-p47 expression plasmid (1.0 μg) followed by transfection with HA-NEMO and HA-IKKβ expression plasmids (0.5 μg). (**d**) HEK293T cells were transfected with expression plasmids encoding NEMO (0.1 μg), HA-IKKβ (0.1 μg) and Flag-p47 (0.1, 0.3 or 1.0 μg). After 48 h, cell lysates were subjected to immunoprecipitation with an anti-HA antibody. (**e**) HEK293T cells were transfected with a control or Flag-p47 expression plasmid. After 48 h, cells were treated with TNF-α (10 ng ml^{-1}). (**f**) HEK293T cells were transfected with control or p97 siRNA. After 24 h, the cells were transfected with NEMO (0.1 μg) and Flag-p47 (0.3 or 1.0 μg) expression plasmids. (**g**) HEK293T cells were transfected with the NEMO expression plasmid (0.1 μg) together with the expression plasmid for Flag-p47 or its various mutants (1 μg). (**h**) HEK293T cells were transfected with expression plasmids encoding NEMO (0.1 μg), Flag-p47 (1.0 μg) and Flag-CYLD (0.1, 0.3 or 1.0 μg). (**i**) HEK293T cells were transfected with 0.1 μg of a pRK5-Flag-NEMO or pRK5-Flag-TRAF6 expression plasmid together with a p47 expression plasmid (0.1, 0.3 or 1.0 μg). After 48 h, the WCL was analysed. The depicted results are representative of three independent experiments.

and the sequence containing the SEP domain and the linker region was also involved, albeit to a lesser extent when compared with the UBA domain (Fig. 6g). Furthermore, CYLD inhibited the p47-mediated reduction of NEMO in a dose-dependent manner (Fig. 6h), indicating that the ubiquitinated form of NEMO is required for the p47-mediated NEMO reduction. However, the

non-ubiquitinated form of NEMO was also reduced in the presence of ubiquitinated NEMO (Fig. 6b), suggesting that the non-ubiquitinated and ubiquitinated forms of NEMO associate with each other and that p47 targets the non-ubiquitinated form of NEMO via ubiquitinated NEMO. As TRAF6 and NEMO become conjugated with Lys63-linked polyubiquitin chains upon stimulation[2,7], we next addressed whether p47 overexpression results in a reduction of TRAF6. HEK293T cells were transfected with an expression plasmid for Flag-NEMO or Flag-TRAF6 in combination with increasing amounts of the Flag-p47 expression plasmid. NEMO expression was reduced by co-expression with p47 even when the lowest amount of the p47 expression plasmid (0.1 μg) was transfected. In contrast, TRAF6 expression was reduced only when the highest amount of the p47 expression plasmid (1.0 μg) was transfected (Fig. 6i). These results suggest that p47 may recognize polyubiquitinated NEMO more efficiently than polyubiquitinated TRAF6. Therefore, p47 is likely to recognize NEMO itself in addition to the polyubiquitin chain conjugated to NEMO. Given that p47 does not bind to non-ubiquitinated NEMO (Fig. 5f,h), the polyubiquitination of NEMO may induce a structural change of NEMO to enable p47 to recognize NEMO itself.

p47 targets ubiquitinated NEMO for lysosomal degradation. To support the hypothesis that p47 induces the degradation of NEMO, p47 and NEMO were co-expressed in HEK293T cells, and the cells were treated with MG132 (a proteasome inhibitor) or E64D in combination with pepstatin A (lysosome inhibitors). NEMO expression was significantly restored in response to treatment with E64D/pepstatin A, but not with MG132 (Fig. 7a), suggesting that p47 induces the lysosomal degradation of polyubiquitinated NEMO. To further confirm the degradation of NEMO under physiological conditions, the TNF-α-induced polyubiquitination of endogenous NEMO was analysed. The enhanced accumulation of polyubiquitinated NEMO was observed in p47-knockdown cells (Fig. 7b) and in the E64D/pepstatin A-treated cells, but not in the MG132-treated cells (Fig. 7c). Similar results were obtained using a different experimental protocol (Supplementary Fig. S4) and with other lysosome inhibitors such as chloroquine and bafilomycin A1 (Supplementary Fig. S5). To demonstrate that NEMO is recruited to the lysosome after TNF-α stimulation, HeLa cells were treated with chloroquine followed by treatment with TNF-α, and the subcellular localization of NEMO and lysosomal-associated membrane protein 1 (LAMP-1), a late endosomal–lysosomal marker, was analysed using confocal immunofluorescence microscopy. A small proportion of NEMO colocalized with LAMP-1 in the lysosome in a TNF-α-stimulation-dependent manner (Fig. 7d). Moreover, chloroquine treatment enhanced TNF-α-induced NF-κB-dependent transcription (Fig. 7e) and interaction of p47 with NEMO (Fig. 7f). Collectively, these results strongly suggest that p47 targets polyubiquitinated NEMO for lysosomal degradation, thereby negatively regulating NF-κB activation.

Potential involvement of p47 in cancer development. Analysis of the Oncomine database[51] revealed that *p47* expression is down-regulated in some human cancers, including prostate carcinoma, glioblastoma and breast carcinoma. In addition, analysis of Gene Expression Omnibus data[52] revealed significant reduction of p47 expression in acute and chronic adult T-cell leukaemia (ATL; Supplementary Fig. S6a), in which the constitutive activation of NF-κB mediated by Tax-dependent and independent mechanisms is crucial in leukemogenesis and survival of tumour cells[53]. On the basis of our preliminary experiments, when compared with non-infected Jurkat T-cell line, p47 expression is significantly reduced at both the mRNA and protein levels in ATL patient-derived and human T-cell leukaemia virus-1-infected cell lines, in which various NF-κB target genes were highly expressed due to constitutive NF-κB activation (Supplementary Fig. S6b,c). Moreover, Tax inhibited the interaction between p47 and the IKK complex, whereas enhanced p47 expression inhibited NF-κB activation in Tax-expressing cells (Supplementary Fig. S6d, e), suggesting that reduced p47 expression may be involved in leukemogenesis. Thus, the altered expression or function of p47 *in vivo* may result in constitutive NF-κB activation, which may trigger development of various cancers.

Discussion

Excess and/or prolonged NF-κB activation leads to the development of inflammatory diseases, autoimmunity and cancer[23–26]. However, it is not fully understood how the amplitude and duration of NF-κB activation are tightly regulated. p47 has previously been identified as an essential factor for the membrane reassembly of the ER, the nuclear envelope and the Golgi apparatus[32–35]. Here we demonstrate that p47 associates with the IKK complex via NEMO within 5 min of stimulation with TNF-α or IL-1. Importantly, the association of p47 with the IKK complex inhibits the stimulation-induced activation of this complex, thereby inhibiting the expression of NF-κB target genes. Thus, p47 is crucial for maintaining appropriate expression levels of cytokines and chemokines, which mediate inflammation.

Several lines of evidence indicate that the negative regulation of IKK by p47 is triggered by the binding of p47 to Lys63-linked or linear polyubiquitin chains that are conjugated to NEMO. First, the inactivation of the UBA domain significantly impairs the p47-mediated inhibition of NF-κB activation. Second, p47 binds to Lys63-linked and linear polyubiquitin chains primarily through its UBA domain. In addition, the binding of p47 to NEMO depends on its UBA domain and polyubiquitin. The co-expression of NEMO with p47 resulted in the degradation of NEMO but not of IKKβ associated with NEMO. This degradation required the UBA domain of p47 and lysosomal proteases but did not require the proteasome. We did not observe a stimulation-dependent degradation of endogenous NEMO, likely because only a small amount of endogenous NEMO is ubiquitinated. However, we did detect a significant level of ubiquitinated NEMO when NEMO was overexpressed. An enhanced TNF-α-induced accumulation of polyubiquitinated endogenous NEMO was observed when p47 was silenced or when cells were treated with lysosomal inhibitors but not with proteasome inhibitors. Moreover, a small but significant portion of NEMO was transferred to the lysosome upon TNF-α stimulation. Given that Shp1, a yeast homologue of p47, binds Atg8, a yeast homologue of LC3 that is required for the elongation of the nascent autophagosome[54], our results suggest that p47 deprives the activated IKK complex of ubiquitinated NEMO and targets ubiquitinated NEMO for lysosomal degradation (Fig. 8). In this sense, p47 is similar to p62 and NBR1, which also each have a UBA domain and target ubiquitinated protein aggregates to autophagosomes via their interaction with LC3 (refs 55,56). However, involvement of autophagic clearance in the p47-mediated NEMO degradation remains to be elucidated.

p47 preferentially binds to Lys63-linked and linear polyubiquitin chains versus Lys48-linked polyubiquitin chains when they contain five or more ubiquitin moieties. As previous studies have shown that the p47 UBA domain binds monoubiquitin[37,39], implying that the native p47 homotrimer should bind three ubiquitin units, the relative positions and orientations of the three UBA domains in the p47 trimer may account for the linkage and length specificities of the p47–polyubiquitin interaction. Interestingly, we found that the sequence containing the SEP domain and the linker region also contribute to ubiquitin binding and IKK inhibition. As the SEP and UBX domains are involved in p47 trimer formation[39], the trimerization of the linker plus the SEP region may result in the formation of a lower-affinity ubiquitin-binding surface that cooperates with the UBA domain to increase the overall polyubiquitin chain affinity.

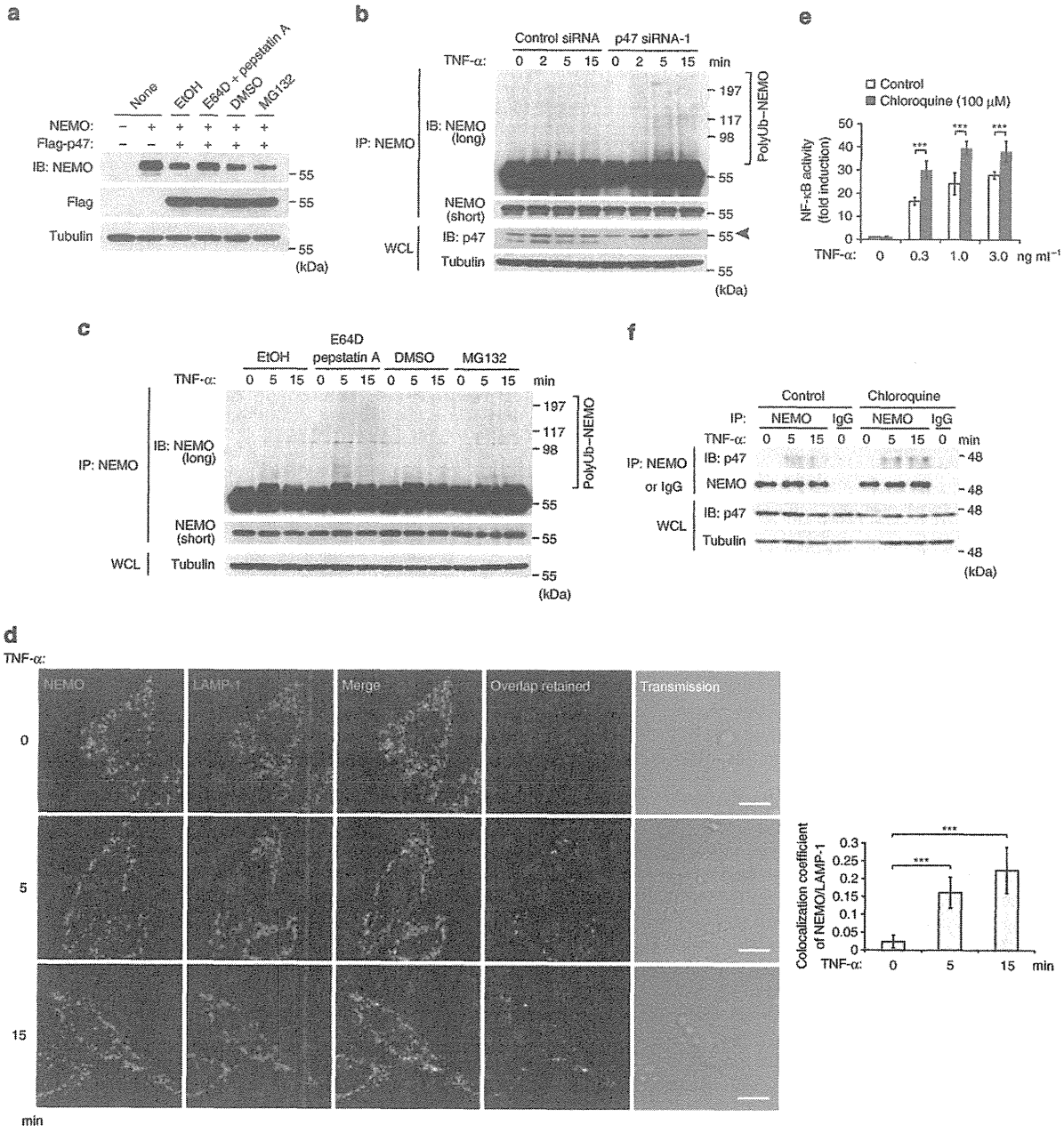

Figure 7 | p47 induces the lysosomal degradation of polyubiquitinated NEMO. (**a**) HEK293T cells were transfected with NEMO (0.1 μg) and Flag-p47 (1 μg) expression plasmids. The cells were treated with E64D (5 μg ml^{-1})/pepstatin A (1 μg ml^{-1}) for 12 h or treated with MG132 (10 μM) for 2 h. (**b**) HeLa cells were transfected with control or p47 siRNA. After TNF-α (10 ng ml^{-1}) stimulation, the cell lysates were subjected to immunoprecipitation with an anti-NEMO antibody followed by immunoblotting with an anti-NEMO antibody. An arrowhead denotes non-specific bands. (**c**) HeLa cells were treated with E64D/pepstatin A for 2 h or with MG132 for 2 h. After TNF-α stimulation, cell lysates were subjected to immunoprecipitation as described in **b**. (**d**) HeLa cells were treated with chloroquine (100 μM) for 2 h. After TNF-α stimulation, the subcellular localization of NEMO and LAMP-1 was analysed using confocal immunofluorescence microscopy. The Manders' colocalization coefficients of NEMO/LAMP-1 were analysed by Olympus imaging software. The results are given as the mean±s.d. (n=30) and are representative of three independent experiments. Scale bar, 10 μm. (**e**) HEK293T cells were transfected with a 3×κB-luc. After 36 h, the cells were untreated or treated with chloroquine for 2 h. After 8 h of TNF-α stimulation, the luciferase activity was measured. The fold induction was calculated by dividing each luciferase activity by that of the control without TNF-α stimulation. The results are given as the mean±s.d. (n=3). (**f**) HeLa cells were treated with chloroquine for 2 h and then stimulated with TNF-α. The cell lysates were subjected to immunoprecipitation with a control IgG or anti-NEMO antibody. The depicted results are representative of three independent experiments. Statistical significance was assessed using a Student's t-test. ***P< 0.01.

The association of p47 with the cytosolic AAA ATPase p97 is crucial for the membrane reassembly of organelles[32]; however, p97 is dispensable for p47-mediated IKK inhibition, suggesting that cytosolic p47 associates with distinct partner proteins, such as LC3 or proteins required for targeting p47 to the autophagosome. The identification of p47-associated proteins in the cytosol is essential

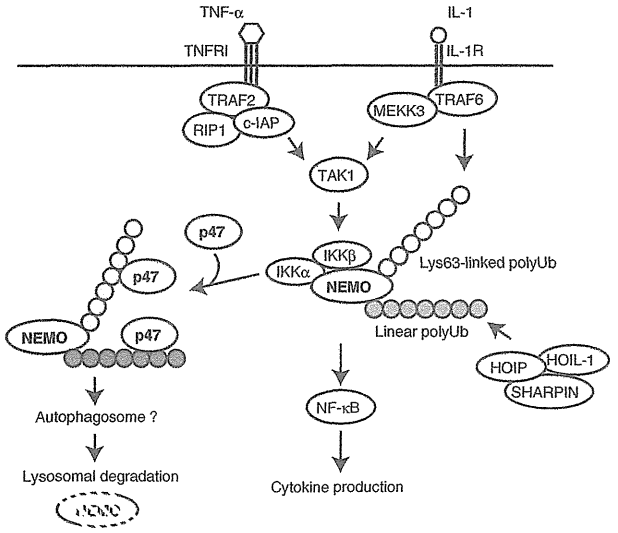

Figure 8 | A model illustrating p47-mediated IKK inhibition. Upon TNF-α and IL-1 stimulation, TRAF6 catalyses the conjugation of Lys63-linked polyubiquitin chains to NEMO, and LUBAC (linear ubiquitin chain assembly complex), which is composed of HOIP, HOIL-1 and SHARPIN, catalyses the conjugation of linear polyubiquitin chains to NEMO. p47 binds to polyubiquitinated NEMO and induces the degradation of NEMO through a lysosome-dependent pathway. Involvement of autophagy in the NEMO degradation remains to be elucidated. PolyUb, polyubiquitin chain.

for understanding how p47 induces the lysosomal degradation of polyubiquitinated NEMO.

DUBs, such as A20 and CYLD, have pivotal roles in the negative regulation of NF-κB activation[27–30]. CYLD is a tumour suppressor protein whose inactivation results in familial cylindromatosis[25]. In contrast, A20-deficient mice develop severe inflammation and cachexia[31]. Although p47 and these DUBs recognize polyubiquitin chains that are generated for NF-κB activation, p47 negatively regulates IKK activation in a manner that is mechanistically distinct from that of A20 and CYLD. It has been proposed that A20 regulates both the initial and termination phases of stimulation-induced NF-κB activation[57–59], whereas CYLD is involved in blocking spontaneous NF-κB activation as well as in the initial phase[25,60]. Given that p47 and these DUBs negatively regulate the initial phase of stimulation-induced NF-κB activation and that CYLD inhibits the interaction of p47 with NEMO, p47 and these two DUBs could cooperatively regulate the initial phase of stimulation-induced NF-κB activation for achieving the appropriate expression levels of NF-κB target genes. Consistent with this idea, significant reduction of p47 expression was observed in ATL cells, which show high levels of constitutive NF-κB activation that protects ATL cells from apoptosis[53]. A better understanding of the mechanisms of p47-mediated IKK inhibition should eventually lead to the development of novel therapeutic approaches that promote the activity of p47.

Methods

Plasmids. Human cDNAs encoding Hsp90, p47 and CYLD were generated by PCR and inserted into the pRK5 vector. The NEMO cDNA was obtained from S Yamaoka (Tokyo Medical and Dental University) and inserted into the pcDNA3 vector (Life Technologies, Carlsbad, CA, USA) or into the pRK5 vector. pRcβact-3HA-IKKα and -IKKβ were obtained from M. Karin (University of California); 3×κB-luc was obtained from S Miyamoto (University of Wisconsin).

Antibodies and reagents. Antibodies used were as follows: anti-p-IκBα (9246), anti-IκBα (9242), anti-p-JNK (9251), anti-p-p38 (9211), anti-p-ERK (9101), anti-IKKα (2682), anti-IKKβ (2684) and anti-NEMO (2695) (Cell Signaling Technology, Danvers, MA, USA); anti-p65 (sc-8008), anti-GST (sc-459), anti-HA-tag (sc-805), anti-CYLD (sc-744435) and anti-ubiquitin (sc-8017) (Santa Cruz Biotechnology, Santa Cruz, USA); anti-Flag M2 (F3165) (Sigma, St Louis, MO, USA); anti-tubulin (CP06) (Millipore, Darmstadt, Germany); anti-p47 (H00055968-B01P) (Abnova, Taipei City, Taiwan); anti-A20 (60-6629-81) (eBioscience, San Diego, CA, USA); anti-p97 (612182) (BD Transduction Laboratories, Franklin Lakes, NJ, USA); and anti-His-tag (PM032) (MBL, Nagoya, Japan). All antibodies were used at a 2,000-fold dilution. Reagents used were as follows: MG132, E64D, and pepstatin A (Peptide Institute, Osaka, Japan) and chloroquine (Wako, Osaka, Japan).

Cell culture and transfection. *A20*$^{-/-}$ MEF was obtained from A. Ma (University of California). *Cyld*$^{-/-}$ MEF was obtained from S. -C. Sun (University of Texas). HEK293T, HeLa and MEF cells were maintained in DMEM supplemented with 10% fetal bovine serum (FBS). Jurkat cells were maintained in RPMI1640 with 10% FBS. Sf9 cells were maintained in Sf900 IIISFM (Life Technologies) supplemented with 10% FBS. The DNA transfection was performed via the calcium phosphate method. siRNAs were transfected using RNAiMAX reagents (Life Technologies). Control siRNA and the following double-stranded siRNAs (Life Technologies) were used: p47-1 sense/anti-sense, 5′-CAACGAGCUGGUGGAUGAUCUCU UU-3′/5′-AAAGAGAUCAUCCACCAGCUCGUUG-3′; p47-2 sense/anti-sense, 5′-GAGAGACCAGUAAACCGAGACCAUU-3′/5′-AAUGGUCUCGGUUUA CUGGUCUCUC-3′; p47-mouse sense/anti-sense, 5′-UGACAUCCUUCAGA GACCUCAUUCA-3′/5′-UGAAUGAGGUCUCUGAAGGAUGUCA-3′; p97-1 sense/anti-sense, 5′-CCCAAGAUGGAUGAAUUGCAGUUGU-3′/5′-ACAA CUGCAAUUCAUCCAUCUUGGG-3′; p97-2 sense/anti-sense, 5′-GGAGUUC AAAGUGGUGGAAACAGAU-3′/5′-AUCUGUUUCCACCACUUUGA ACUCC-3′.

Mass spectrometry. Jurkat cells expressing Flag-NEMO were suspended in hypotonic buffer (10 mM Tris–HCl at pH 7.4, 1.5 mM $MgCl_2$, 10 mM KCl, 0.5 mM dithiothreitol (DTT) and protease inhibitor cocktail (Roche, Basel, Switzerland)), and then lysed with a Dounce homogenizer. Cell debris was removed by ultracentrifugation at 100,000*g* for 1 h to prepare the S-100 cytosolic fraction. Recombinant Tax protein was added to the S-100 fraction, and the resultant reaction mixture was incubated at 30 °C for 1 h. Protein complexes containing NEMO were then immunoprecipitated using an anti-Flag antibody and were eluted with Flag peptides. The eluted proteins were digested with trypsin and loaded onto an automated nanoflow liquid chromatography system (Dina; KYA Technologies, Tokyo, Japan) coupled to a quadrupole time-of-flight tandem mass spectrometer (Q-Star Elite; AB SCIEX, Framingham, MA, USA). The tandem mass spectrometry signals were processed against human protein sequences in the NCBI RefSeq database using the Mascot algorithm (Matrix Science, Boston, MA, USA).

Immunoprecipitation and immunoblot analysis. For immunoprecipitation, cells were lysed in TNE buffer (20 mM Tris–HCl at pH 7.5, 150 mM NaCl, 2 mM EDTA, 1 mM $MgCl_2$, 10 mM NaF, 1% (v/v) NP-40, 10 mM β-glycerophosphate, 1 mM Na_3VO_4, 1 mM DTT, 5 mM *N*-ethylmaleimide, protease inhibitor cocktail) and centrifuged at 22,000*g* for 15 min at 4 °C to remove the insoluble fraction. The supernatants were incubated with 0.5 μg of antibody plus 10 μl of protein G-sepharose (GE Healthcare, Piscataway, NJ, USA). The immunoprecipitates were washed three times and subjected to immunoblotting. For immunoblot analysis, immunoprecipitates or whole-cell lysates were separated by SDS–PAGE and transferred to polyvinylidenedifluoride membranes (Immobilon P, Millipore). The membranes were then incubated with the primary antibodies. Immunoreactive proteins were visualized with anti-rabbit or anti-mouse IgG conjugated to horseradish peroxidase (GE Healthcare) followed by processing with an ECL detection system (GE Healthcare).

Luciferase reporter assay. HEK293T cells were transfected with the plasmids encoding wild type or various p47 mutants together with 20 ng of luciferase reporter (3×κB-luc) and 30 ng of β-actin–β-galactosidase plasmid. After 24 h of incubation, the cells were treated with TNF-α for 24 h, and the luciferase activity was measured using the Luciferase Assay System (Toyo Ink, Tokyo, Japan). β-galactosidase activity was used to normalize the transfection efficiency. In some experiments, siRNAs were transfected 24 h before plasmid transfection.

***In vitro* IKK kinase assay.** HEK293T cells were treated with TNF-α (10 ng ml^{-1}) for the indicated times and lysed in TNE buffer without *N*-ethylmaleimide. IKK complexes were immunoprecipitated with an anti-NEMO antibody. The immunoprecipitates were incubated at 30 °C for 1 h in kinase buffer (50 mM Tris–HCl at pH 7.5, 5 mM $MgCl_2$, 2 mM ATP, 10 mM creatine phosphate, 3.5 U ml^{-1} creatine kinase, 5 mM NaF, 20 mM β-glycerophosphate and 1 mM Na_3VO_4) with 100 ng of GST-IκBα (amino acids 1–54). The reaction mixtures were subjected to immunoblotting using an anti-p-IκBα antibody, and the intensities of the bands were quantified using ImageJ software (National Institutes of Health).

Electrophoretic mobility shift assay. HeLa cells were stimulated with TNF-α or IL-1 and then suspended in hypotonic buffer. The cell suspensions were incubated

on ice for 30 min and centrifuged at 22,000*g* for 5 min at 4 °C. The nuclear pellets were suspended in extraction buffer (20 mM HEPES at pH 7.9, 420 mM NaCl, 1.5 mM $MgCl_2$, 0.2 mM EDTA, 0.5 mM DTT, 25% (v/v) glycerol and a protease inhibitor cocktail) and incubated on ice for 20 min. The nuclear extracts were obtained from the supernatants. The nuclear extracts (3 μg) were incubated with ^{32}P-labelled oligonucleotides that contained the NF-κB-binding site or the Oct-1-binding site for 25 min at 25 °C. The DNA–protein complexes were separated by electrophoresis with a 4% polyacrylamide gel. The following oligonucleotides were used: NF-κB, 5′-AGCTTCAGAGGGGACTTTCCGAGAGG-3′, and 5′-TCGA CCTCTCGGAAAGTCCCCTCTGA-3′; and Oct-1, 5′-TGTCGAATGCAAATC ACTAGAA-3′ and 5′-TGTTCTAGTGATTTGCATTCGA-3′.

Quantitative real-time reverse transcriptase PCR assays. The total RNA was isolated from TNF-α- or IL-1-treated HeLa cells with Trizol reagent (Life Technologies). cDNA was synthesized from 1 μg of total RNA with Prime Script II (Takara Bio, Shiga, Japan). Quantitative real-time PCR analysis was performed on a 7300 Fast Real-Time PCR System (Life Technologies) using FastStart Universal SYBR Green Master (Roche). The level of β-actin expression was used to normalize the data. The following primers were used: IL-8 sense/anti-sense, 5′-ATGACTT CCAAGCTGGCCGT-3′/5′-TTACATAATTTCTGTGTTGGC-3′; TNF-α sense/anti-sense, 5′-GGAGAAGGGTGACCGACTCA-3′/5′-TGCCCAGAC TCGGCAAAG-3′; β-actin sense/anti-sense, 5′-TTCTACAATGAGCTGCGT GTG-3′/5′-CCTTAATGTCACGCACGATTT-3′.

Recombinant proteins. His_6-tagged p47, NEMO, TRAF6, cIAP1 and Tax were produced using the Bac-to-Bac Baculovirus Expression System (Life Technologies). Briefly, a 50-ml culture of Sf9 cells (1×10^6 cells ml^{-1}) was infected with recombinant baculovirus expressing each protein. Seventy-two hours after infection, cells were harvested, and His_6-tagged recombinant proteins were purified using Ni-NTA resin (QIAGEN, Valencia, CA, USA). His_6-UBE1, His_6-UbcH13/Uev1a, UbcH5c, and ubiquitin (wild-type, K63 only, K48 only) were purchased (Boston Biochem, Cambridge, MA, USA).

***In vitro* binding assays of p47 and polyubiquitinated NEMO.** In Figure 5f, the reactions were performed at 37 °C for 2 h in 50 μl of kinase buffer containing 1 μg of His_6-UBE1, 2 μg of His_6-UbcH13/Uev1a, 2 μg of His_6-TRAF6, 1 μg of His_6-NEMO and 50 μg of ubiquitin. In Figure 5g, the reactions were performed at 37 °C for 2 h in 25 μl of kinase buffer containing 0.5 μg of UBE1, 0.85 μg of UbcH5c, 0.2 μg of His_6-cIAP1, 0.5 μg of His_6-NEMO and 5 μg of ubiquitin containing only Lys-48 or only Lys-63. After incubation, the reaction mixtures were incubated with 1 μg of an anti-NEMO antibody together with 10 μl of protein G-sepharose. The immunoprecipitates were incubated with recombinant His_6-p47 or its mutants at 4 °C for 2 h. After washing, His_6-p47 or its mutants bound to the immunoprecipitates were analysed by immunoblotting.

***In vitro* binding assays of p47 and polyubiquitin chains.** Ni-NTA resin was incubated with 10 μg of p47 and its mutants at 4 °C for 2 h in binding buffer (20 mM Tris–HCl at pH 7.5, 150 mM NaCl, 0.5% (v/v) NP-40, 2.5 mg ml^{-1} BSA, 20 mM imidazole and 5 mM 2-mercaptoethanol). The beads were then incubated with 1.0 μg of linear (Enzo Lifescience, Farmingdale, NY, USA), Lys63-, or Lys48-linked polyubiquitin chains (Boston Biochem) at 4 °C for 2 h. After incubation, the beads were washed and subjected to immunoblotting.

Immunofluorescence. HeLa cells were treated with chloroquine (100 μM) for 2 h. After TNF-α stimulation, the cells were washed with PBS and fixed in 4% paraformaldehyde followed by permeabilization with 1% NP-40. The cells were then incubated with primary antibodies for 1 h followed by incubation with secondary antibodies for 1 h. The localization of NEMO and LAMP-1 was analysed using a confocal laser-scanning microscope FV100-D (Olympus, Tokyo, Japan). The following antibodies were used: anti-NEMO (sc-8032) and anti-LAMP-1 (sc-5570) (Santa Cruz Biotechnology), Alexa Fluor 488 goat anti-mouse IgG (A11029) and Alexa Fluor 546 goat anti-rabbit IgG (A11035) (Life Technologies). Images in two channels were acquired by sequential scanning. For quantification, a region of interest was defined around an individual cell ($n=30$), and the Manders' colocalization coefficients were determined under the same threshold values using FV10-ASW imaging software (Olympus).

Statistics. Statistically significant differences between the mean values were determined using Student's *t*-test (***$P<0.01$, **$P<0.02$ and *$P<0.05$). Data are presented as the means±s.d.

References

1. Iwai, K. & Tokunaga, F. Linear polyubiquitination: a new regulator of NF-κB activation. *EMBO Rep.* **10,** 706–713 (2009).
2. Gautheron, J. & Courtois, G. 'Without Ub I am nothing': NEMO as a multifunctional player in ubiquitin-mediated control of NF-κB activation. *Cell. Mol. Life Sci.* **67,** 3101–3113 (2010).
3. Liu, S. & Chen, Z. J. Expanding role of ubiquitination in NF-κB signaling. *Cell Res.* **21,** 6–21 (2011).
4. Hayden, M. S. & Ghosh, S. Shared principles in NF-κB signaling. *Cell* **132,** 344–362 (2008).
5. Sun, S. C. Controlling the fate of NIK: a central stage in noncanonical NF-κB signaling. *Sci. Signal.* **3,** pe18 (2010).
6. Xia, Z. P. *et al.* Direct activation of protein kinases by unanchored polyubiquitin chains. *Nature* **461,** 114–119 (2009).
7. Lamothe, B. *et al.* Site-specific Lys-63-linked tumor necrosis factor receptor-associated factor 6 auto-ubiquitination is a critical determinant of IκB kinase activation. *J. Biol. Chem.* **282,** 4102–4112 (2007).
8. Yamazaki, K. *et al.* Two mechanistically and temporally distinct NF-κB activation pathways in IL-1 signaling. *Sci. Signal.* **2,** ra66 (2009).
9. Deng, L. *et al.* Activation of the IκB kinase complex by TRAF6 requires a dimeric ubiquitin-conjugating enzyme complex and a unique polyubiquitin chain. *Cell* **103,** 351–361 (2000).
10. Kanayama, A. *et al.* TAB2 and TAB3 activate the NF-κB pathway through binding to polyubiquitin chains. *Mol. Cell* **15,** 535–548 (2004).
11. Laplantine, E. *et al.* NEMO specifically recognizes K63-linked poly-ubiquitin chains through a new bipartite ubiquitin-binding domain. *EMBO J.* **28,** 2885–2895 (2009).
12. Wang, C. *et al.* TAK1 is a ubiquitin-dependent kinase of MKK and IKK. *Nature* **412,** 346–351 (2001).
13. Mahoney, D. J. *et al.* Both cIAP1 and cIAP2 regulate TNFα-mediated NF-κB activation. *Proc. Natl Acad. Sci. USA* **105,** 11778–11783 (2008).
14. Bertrand, M. J. *et al.* cIAP1 and cIAP2 facilitate cancer cell survival by functioning as E3 ligases that promote RIP1 ubiquitination. *Mol. Cell* **30,** 689–700 (2008).
15. Xu, M., Skaug, B., Zeng, W. & Chen, Z. J. A ubiquitin replacement strategy in human cells reveals distinct mechanisms of IKK activation by TNFα and IL-1β. *Mol. Cell* **36,** 302–314 (2009).
16. Ni, C. Y. *et al.* Cutting edge: K63-linked polyubiquitination of NEMO modulates TLR signaling and inflammation *in vivo*. *J. Immunol.* **180,** 7107–7111 (2008).
17. Sebban-Benin, H. *et al.* Identification of TRAF6-dependent NEMO polyubiquitination sites through analysis of a new NEMO mutation causing incontinentia pigmenti. *Hum. Mol. Genet.* **16,** 2805–2815 (2007).
18. Abbott, D. W., Wilkins, A., Asara, J. M. & Cantley, L. C. The Crohn's disease protein, NOD2, requires RIP2 in order to induce ubiquitinylation of a novel site on NEMO. *Curr. Biol.* **14,** 2217–2227 (2004).
19. Tokunaga, F. *et al.* Involvement of linear polyubiquitylation of NEMO in NF-κB activation. *Nat. Cell Biol.* **11,** 123–132 (2009).
20. Gerlach, B. *et al.* Linear ubiquitination prevents inflammation and regulates immune signalling. *Nature* **471,** 591–596 (2011).
21. Ikeda, F. *et al.* SHARPIN forms a linear ubiquitin ligase complex regulating NF-κB activity and apoptosis. *Nature* **471,** 637–641 (2011).
22. Tokunaga, F. *et al.* SHARPIN is a component of the NF-κB-activating linear ubiquitin chain assembly complex. *Nature* **471,** 633–636 (2011).
23. Yamamoto, Y. & Gaynor, R. B. Role of the NF-κB pathway in the pathogenesis of human disease states. *Curr. Mol. Med.* **1,** 287–296 (2001).
24. Tak, P. P. & Firestein, G. S. NF-κB: a key role in inflammatory diseases. *J. Clin. Invest.* **107,** 7–11 (2001).
25. Sun, S. C. CYLD: a tumor suppressor deubiquitinase regulating NF-κB activation and diverse biological processes. *Cell Death Differ.* **17,** 25–34 (2010).
26. Inoue, J., Gohda, J., Akiyama, T. & Semba, K. NF-κB activation in development and progression of cancer. *Cancer Sci* **98,** 268–274 (2007).
27. Wertz, I. E. *et al.* De-ubiquitination and ubiquitin ligase domains of A20 downregulate NF-κB signalling. *Nature* **430,** 694–699 (2004).
28. Kovalenko, A. *et al.* The tumour suppressor CYLD negatively regulates NF-κB signalling by deubiquitination. *Nature* **424,** 801–805 (2003).
29. Trompouki, E. *et al.* CYLD is a deubiquitinating enzyme that negatively regulates NF-κB activation by TNFR family members. *Nature* **424,** 793–796 (2003).
30. Komander, D. *et al.* Molecular discrimination of structurally equivalent Lys 63-linked and linear polyubiquitin chains. *EMBO Rep.* **10,** 466–473 (2009).
31. Malynn, B. A. & Ma, A. A20 takes on tumors: tumor suppression by an ubiquitin-editing enzyme. *J. Exp. Med.* **206,** 977–980 (2009).
32. Kondo, H. *et al.* p47 is a cofactor for p97-mediated membrane fusion. *Nature* **388,** 75–78 (1997).
33. Patel, S. & Latterich, M. The AAA team: related ATPases with diverse functions. *Trends Cell Biol.* **8,** 65–71 (1998).
34. Roy, L. *et al.* Role of p97 and syntaxin 5 in the assembly of transitional endoplasmic reticulum. *Mol. Biol. Cell* **11,** 2529–2542 (2000).
35. Hetzer, M. *et al.* Distinct AAA-ATPase p97 complexes function in discrete steps of nuclear assembly. *Nat. Cell Biol.* **3,** 1086–1091 (2001).
36. Shibata, Y., Tanaka, Y., Gohda, J. & Inoue, J. Activation of the IκB kinase complex by HTLV-1 Tax requires cytosolic factors involved in Tax-induced polyubiquitination. *J. Biochem.* **150,** 679–686 (2011).
37. Meyer, H. H., Wang, Y. & Warren, G. Direct binding of ubiquitin conjugates by the mammalian p97 adaptor complexes, p47 and Ufd1-Npl4. *EMBO J.* **21,** 5645–5652 (2002).

38. Schuberth, C., Richly, H., Rumpf, S. & Buchberger, A. Shp1 and Ubx2 are adaptors of Cdc48 involved in ubiquitin-dependent protein degradation. *EMBO Rep.* **5,** 818–824 (2004).
39. Yuan, X. *et al.* Structure, dynamics and interactions of p47, a major adaptor of the AAA ATPase, p97. *EMBO J.* **23,** 1463–1473 (2004).
40. Hartmann-Petersen, R. *et al.* The Ubx2 and Ubx3 cofactors direct Cdc48 activity to proteolytic and nonproteolytic ubiquitin-dependent processes. *Curr. Biol.* **14,** 824–828 (2004).
41. Wojcik, C., Yano, M. & DeMartino, G. N. RNA interference of valosin-containing protein (VCP/p97) reveals multiple cellular roles linked to ubiquitin/proteasome-dependent proteolysis. *J. Cell Sci.* **117,** 281–292 (2004).
42. Uchiyama, K. *et al.* The localization and phosphorylation of p47 are important for Golgi disassembly-assembly during the cell cycle. *J. Cell Biol.* **161,** 1067–1079 (2003).
43. Yamamoto, M. *et al.* Key function for the Ubc13 E2 ubiquitin-conjugating enzyme in immune receptor signaling. *Nat. Immunol.* **7,** 962–970 (2006).
44. Zhong, H., Voll, R. E. & Ghosh, S. Phosphorylation of NF-κB p65 by PKA stimulates transcriptional activity by promoting a novel bivalent interaction with the coactivator CBP/p300. *Mol. Cell* **1,** 661–671 (1998).
45. Hofmann, K. & Bucher, P. The UBA domain: a sequence motif present in multiple enzyme classes of the ubiquitination pathway. *Trends Biochem. Sci.* **21,** 172–173 (1996).
46. Buchberger, A., Howard, M. J., Proctor, M. & Bycroft, M. The UBX domain: a widespread ubiquitin-like module. *J. Mol. Biol.* **307,** 17–24 (2001).
47. Kaneko, Y., Tamura, K., Totsukawa, G. & Kondo, H. Isolation of a point-mutated p47 lacking binding affinity to p97ATPase. *FEBS Lett.* **584,** 3873–3877 (2010).
48. Wojcik, C. *et al.* Valosin-containing protein (p97) is a regulator of endoplasmic reticulum stress and of the degradation of N-end rule and ubiquitin-fusion degradation pathway substrates in mammalian cells. *Mol. Biol. Cell* **17,** 4606–4618 (2006).
49. Kang, R. S. *et al.* Solution structure of a CUE-ubiquitin complex reveals a conserved mode of ubiquitin binding. *Cell* **113,** 621–630 (2003).
50. Tang, E. D., Wang, C. Y., Xiong, Y. & Guan, K. L. A role for NF-κB essential modifier/IκB kinase-γ (NEMO/IKKγ) ubiquitination in the activation of the IκB kinase complex by tumor necrosis factor-α. *J. Biol. Chem.* **278,** 37297–37305 (2003).
51. Rhodes, D. R. *et al.* Oncomine 3.0: genes, pathways, and networks in a collection of 18,000 cancer gene expression profiles. *Neoplasia* **9,** 166–180 (2007).
52. Yamagishi, M. *et al.* Polycomb-mediated loss of miR-31 activates NIK-dependent NF-κB pathway in adult T cell leukemia and other cancers. *Cancer Cell* **21,** 121–135 (2012).
53. Watanabe, M. *et al.* Dual targeting of transformed and untransformed HTLV-1-infected T cells by DHMEQ, a potent and selective inhibitor of NF-κB, as a strategy for chemoprevention and therapy of adult T-cell leukemia. *Blood* **106,** 2462–2471 (2005).
54. Krick, R. *et al.* Cdc48/p97 and Shp1/p47 regulate autophagosome biogenesis in concert with ubiquitin-like Atg8. *J. Cell Biol.* **190,** 965–973 (2010).
55. Kirkin, V. *et al.* A role for NBR1 in autophagosomal degradation of ubiquitinated substrates. *Mol. Cell* **33,** 505–516 (2009).
56. Komatsu, M. *et al.* Homeostatic levels of p62 control cytoplasmic inclusion body formation in autophagy-deficient mice. *Cell* **131,** 1149–1163 (2007).
57. Skaug, B. *et al.* Direct, noncatalytic mechanism of IKK inhibition by A20. *Mol. Cell* **44,** 559–571 (2011).
58. Lee, E. G. *et al.* Failure to regulate TNF-induced NF-κB and cell death responses in A20-deficient mice. *Science* **289,** 2350–2354 (2000).
59. Shembade, N., Ma, A. & Harhaj, E. W. Inhibition of NF-κB signaling by A20 through disruption of ubiquitin enzyme complexes. *Science* **327,** 1135–1139 (2010).
60. Reiley, W. W. *et al.* Deubiquitinating enzyme CYLD negatively regulates the ubiquitin-dependent kinase Tak1 and prevents abnormal T cell responses. *J. Exp. Med.* **204,** 1475–1485 (2007).

Acknowledgements

We thank M. Karin for IKKα/β expression plasmids, S. Miyamoto for 3×κB-luc reporter, S. Yamaoka for NEMO cDNA, A. Ma for *A20*$^{-/-}$ MEF, S. -C. Sun for *Cyld*$^{-/-}$ MEF, T. Akiyama and N. Yamaguchi for helpful discussions, and K. Shimizu, S. Okada and K. Miyazaki for secretarial assistance. This work was supported in part by a grant-in-aid for Scientific Research on Innovative Areas and by a contract research fund for Program of Japan Initiative for Global Research Network on Infectious Diseases from the Ministry of Education, Culture, Sports, Science and Technology of Japan (J-i.I.), by the Takada Science Foundation (J-i.I.), and by the Fugaku Trust for Medicinal Research (J-i.I.).

Author contributions

All authors contributed to the experimental design and data interpretation. Y.S., M.O., H.K.-H., X.H. and Y.T. carried out the experiments. Y.S., J.G., and J-i.I. planned the project. Y.S. and J-i.I. wrote the paper.

Additional information

Supplementary Information accompanies this paper at http://www.nature.com/naturecommunications

Competing financial interests: The authors declare no competing financial interests.

Reprints and permission information is available online at http://npg.nature.com/reprintsandpermissions/

How to cite this article: Shibata, Y. *et al.* p47 negatively regulates IKK activation by inducing the lysosomal degradation of polyubiquitinated NEMO. *Nat. Commun.* 3:1061 doi: 10.1038/ncomms2068 (2012).

Cancer Science
The official journal of the Japanese Cancer Association JCA

Tax is a potential molecular target for immunotherapy of adult T-cell leukemia/lymphoma

Susumu Suzuki,[1,2,8] Ayako Masaki,[1,8] Takashi Ishida,[1,7] Asahi Ito,[1] Fumiko Mori,[1] Fumihiko Sato,[1,3] Tomoko Narita,[1] Masaki Ri,[1] Shigeru Kusumoto,[1] Hirokazu Komatsu,[1] Yasuo Fukumori,[4] Hiroyoshi Nishikawa,[5] Yuetsu Tanaka,[6] Akio Niimi,[1] Hiroshi Inagaki,[3] Shinsuke Iida[1] and Ryuzo Ueda[2]

[1]Department of Medical Oncology & Immunology, Nagoya City University Graduate School of Medical Sciences, Nagoya; [2]Department of Tumor Immunology, Aichi Medical University School of Medicine, Nagakute; [3]Department of Clinical Pathology, Nagoya City University Graduate School of Medical Sciences, Nagoya; [4]Osaka Blood Center, Osaka; [5]Experimental Immunology, Immunology Frontier Research Center, Osaka University, Osaka; [6]Department of Immunology, Graduate School of Medicine, Ryukyu University, Nishihara, Japan

(Received May 13, 2012/Revised June 18, 2012/Accepted June 21, 2012/Accepted manuscript online June 26, 2012/Article first published online August 12, 2012)

We expanded CTL specific for Tax (a human T-lymphotropic virus type-1-encoded gene product) *in vitro* from PBMC of several adult T-cell leukemia/lymphoma (ATL) patients, and document its potential significance as a target for ATL immunotherapy. Tax-specific CTL responses against tumor cells were restricted by Tax-expression and the appropriate human leukocyte antigen (HLA) type. Tax-specific CTL recognized HLA/Tax-peptide complexes on autologous ATL cells, even when their Tax expression was so low that it could only be detected by RT-PCR but not by flow cytometry. Recognition resulted in interferon gamma (IFN-γ) production and target cell lysis. This would be the first report that Tax-specific CTL from ATL patients specifically recognized and killed autologous tumor cells that expressed Tax. The Tax-specific CTL responded to as little as 0.01 pM of the corresponding peptide, indicating that their T-cell receptor avidity was much higher than that of any other CTL recognizing viral or other tumor antigens. This is presumably the reason why the Tax-specific CTL recognized and killed autologous ATL cells despite their very low Tax expression. In addition, cell cycle analyses and experiments with primary ATL cell-bearing mice demonstrated that ATL cells present at the site of active cell proliferation, such as in the tumor masses, expressed substantial amounts of Tax, but it was minimally expressed by the tumor cells in a quiescent state, such as in the blood. The present study not only provides a strong rationale for exploiting Tax as a possible target for ATL immunotherapy but also contributes to our understanding of the immunopathogenesis of ATL. (*Cancer Sci* 2012; 103: 1764–1773)

Adult T-cell leukemia/lymphoma (ATL) is a distinct hematologic malignancy caused by human T-lymphotropic virus type 1 (HTLV-1).[1,2] ATL has a long latency period of 50–60 years, so affected individuals have usually been exposed to HTLV-1 early in their lives via agents including infected lymphocytes, mainly from mother's breast milk.[3,4] Only small subpopulations (approximately 5%) of HTLV-1-infected individuals progress to ATL, but there are no clear biomarkers separating those who will develop ATL from those who remain asymptomatic carriers (AC).[2] There are four clinical subtypes of ATL: acute, lymphoma, chronic and smoldering.[5] The two former types have more aggressive clinical courses (aggressive variants), while the latter are less aggressive (indolent variants).

Human T-lymphotropic virus type 1 Tax, a virus-encoded regulatory gene product, is required for the virus to transform cells,[6] and is thought to be indispensable for oncogenesis. Therefore, Tax has been considered as a molecular target for immunotherapy against ATL, and many such investigations have been published.[7–10] However, it has been reported that the level of Tax expression in HTLV-1-infected cells decreases during disease progression, and *Tax* transcripts are detected only in approximately 40% of established ATL cases.[11] Moreover, weak or absent responses to Tax have been observed in ATL patients,[12] leading to controversy as to whether Tax is an appropriate target for immunotherapy of ATL. In the present study, we expanded Tax-specific CTL *in vitro* from PBMC of several ATL patients, and tested their ability to respond to several ATL cell lines, HTLV-1-immortalized lines and to autologous ATL cells. The aim was to clarify the involvement of Tax-specific CTL (Tax-CTL) in the immunopathogenesis of ATL, and to confirm the significance of Tax as a potential immunotherapeutic target in ATL.

Materials and Methods

Primary adult T-cell leukemia/lymphoma cells. Primary ATL cells were separated from PBMC using anti-human CD4 microbeads (Miltenyi Biotec, Bergisch Gladbach, Germany). All donors provided informed written consent before sampling according to the Declaration of Helsinki, and the present study was approved by the institutional ethics committees of Nagoya City University Graduate School of Medical Sciences.

Cell lines. TL-Su and TL-Om1 were provided by the Cell Resource Center for Biomedical Research, Tohoku University (Sendai, Japan). TCL-Kan was kindly provided by Professor Mari Kannagi (Tokyo Medical and Dental University, Tokyo, Japan).[13] HUT102, ATN-1, MT-2 and MT-1 have been previously described.[14,15] MT-4 was purchased from the Health Science Research Resources Bank (Osaka, Japan). HUT102, ATN-1, MT-1 and TL-Om1 are ATL cell lines, and TL-Su, TCL-Kan, ILT-#37, MT-2 and MT-4 are HTLV-I-immortalized lines. K562 is the chronic myelogenous leukemia blast crisis cell line.[16]

Human leukocyte antigen typing. Genotyping of HLA-A, B and C was performed using an HLA-typing Kit (WAKFlow HLA-typing kit, WAKUNAGA Pharmacy, Hiroshima, Japan).

Expansion of human T-lymphotropic virus type 1 Tax-specific CTL. PBMC from ATL patients or HTLV-1 AC were suspended in RPMI-1640 supplemented with 10% autologous plasma and 0.1 μM of the corresponding Tax epitope peptides (LLFGYPVYV or SFHSLHLLF) at a cell concentration of 2.0×10^6/mL. These two synthetic peptides were purchased from Invitrogen (Carlsbad, CA, USA). The cell suspension was cultured at 37°C in 5%CO_2 for 2 days, and then an equal volume of RPMI-1640 supplemented with 100 IU/mL of IL-2

[7]To whom correspondence should be addressed.
E-mail: itakashi@med.nagoya-cu.ac.jp
[8]These authors contributed equally to this work.

doi: 10.1111/j.1349-7006.2012.02371.x

was added. After subsequent culture for 5 days, an equal volume of ALyS505N (Cell Science & Technology Institute, Sendai, Japan) supplemented with 100 IU/mL of IL-2 was added, and the cells were cultured with appropriate medium (ALyS505N with 100 IU/mL of IL-2) for 7 days. Cytomegalovirus (CMV)-pp65 specific CTL were expanded in the same manner using peptides such as NLVPMVATV or QYDPVAALF (Invitrogen). Viable cell counts were determined using the trypan blue assay.

Antibodies, tetramers and flow cytometry. Phycoerythrin-conjugated HLA-A*02:01/Tax11–19 (LLFGYPVYV), HLA-A*24:02/Tax301–309 (SFHSLHLLF), HLA-A*02:01/pp65 495–503 (NLVPMVATV) and HLA-A*24:02/pp65 341–349 (QYDPVAALF) tetramers, and phycoerythrin-Cyanin5-conjugated anti-CD8 monoclonal antibody (mAb) were purchased from Medical & Biological Laboratories, Nagoya, Japan. Allophycocyanin-conjugated anti-human CD45 mAb (2D1) and PerCP-conjugated anti-CD4 mAb (SK3) were purchased from BD Biosciences (San Jose, CA, USA). Tax expression was assessed by FITC-conjugated anti-Tax mAb Lt-4.[17] FITC-conjugated anti-interferon gamma (IFN-γ) mAb (45.15) was purchased from Medical & Biological Laboratories. Cell cycle assessments were performed by BrdU Flow Kits (BD Biosciences). Cells were analyzed on a FACSCalibur (BD Biosciences) with the aid of FlowJo software (Tree Star, Ashland, OR, USA).

CTL assay. Cytotoxic activity was determined by a standard 4-h chromium^{51} release assay as previously described.[18] All values given are means of triplicate determinations.

Quantitative RT-PCR. *Tax*, *human CD4* and *β-actin* mRNA were amplified as previously described.[19] The primer set for Tax was as follows: sense, 5′-AAGACCACCAACACCA TGGC-3′; and antisense, 5′-CCAAACACGTAGACTGGGTAT CC-3′.

Animals. NOD/Shi-*scid*, IL-2Rγ^{null} (NOG) mice were purchased from the Central Institute for Experimental Animals (Kawasaki, Japan). All of the *in vivo* experiments were approved by the Ethics Committee of the Center for Experimental Animal Science, Nagoya City University Graduate School of Medical Sciences.

Results

Expansion of Tax-specific CTL. Expansion of Tax-CTL was performed by stimulating PBMC from 14 ATL patients and 6 HTLV-1 AC with synthetic peptides. PBMC from patients 1, 2, 3, 6, 8, 9 and 13 were stimulated with Tax11–19, and those from patients 4, 5, 7, 10, 11, 12 and 14 with Tax301–309 (Tables 1 and 2). Patients 1–6 were all in complete remission (CR) at the time of blood sampling. Patient 1 had achieved CR after allogeneic hematopoietic stem cell transplantation (HSCT) 5 years previously, patients 2 and 3 after systemic chemotherapy and anti-CCR4 mAb treatment,[20,21] patient 4 after systemic chemotherapy alone, and patient 5 after allogeneic HSCT 9 months earlier (and was receiving FK506 at the time of sampling). Finally, patient 6 achieved CR after systemic chemotherapy and anti-CCR4 mAb treatment, and was receiving prednisolone at the time of sampling. As shown in Table 1, Tax-CTL could be expanded *in vitro* (fold expansion >10) by stimulation with Tax peptide in 13 of 17 ATL cases. With respect to HTLV-1 AC, we confirmed efficient expansion (fold expansion >10^2) of Tax-CTL from six of six individuals using Tax11–19 or Tax301–309 peptides in the same manner (data not shown), which are consistent with a previous report.[22] Although the degree of expansion of Tax-CTL varied among the ATL patients, there was a trend for higher rates in PBMC from those with indolent variant ATL not on any systemic treatment, or from patients with aggressive ATL in treatment-induced remission, compared to lower or absent expansion in patients initially diagnosed with an aggressive variant. In particular, patient 8 progressed from chronic to acute subtype during the present study. Tax-CTL could be efficiently expanded from this patient during the chronic phase, but no longer after progression to acute subtype. This was despite the finding that the percentage of HLA-A*02:01/Tax11–19 tetramer-positive cells in the PBMC was almost the same as before disease progression (Fig. 1). These observations collectively indicate that insufficient responses to Tax observed in ATL patients, which are also reported by other investigators,[12,23,24] are related to disease progression from indolent to aggressive clinical variants. Subsequently, patient 8 received systemic chemotherapy but failed to achieve CR. He then received allogeneic HSCT with reduced intensity conditioning and entered partial remission. At this time, when he was not receiving immunosuppression after HSCT, his Tax-CTL could again be efficiently expanded from PBMC. This indicates that substantial anti-Tax responses can be restored by appropriate anti-ATL therapies, when the patient is brought from active ATL into remission (Fig. 1). Even though patients were in CR, immunosuppressive agents such as FK506 or prednisolone were likely to have prevented CTL expansions, as observed in patients 5 and 6, consistent with reports that HTLV-1 AC liver transplant recipients developed ATL under immunosuppression.[25,26] In patient 14, the Tax-CTL expansion rate was drastically increased by depletion of CD4+ cells, most of which consisted of the ATL cells themselves. This suggests that Tax-specific immune responses were suppressed by the tumor cells, consistent with our previous report that ATL cells from a subgroup of patients functioned as regulatory T (Treg) cells.[27]

T-cell receptor avidity of the expanded Tax-specific CTL. Specific IFN-γ production following stimulation with serial concentrations (0.01–100 pM) of Tax11–19 or Tax301–309 peptides was used as a readout to measure the T-cell receptor (TCR) avidity of the expanded Tax-CTL. Intracellular IFN-γ was clearly detected specifically even at a peptide concentration of 0.01 pM in both HLA-A*02:01-restricted Tax-CTL from patient 1 (Fig. 2A) and HLA-A*24:02-restricted Tax-CTL from patient 7 (Fig. 2B). We also analyzed the TCR avidity of CMV-pp65-specific CTL expanded from the same patients. Specific IFN-γ production by HLA-A*02:01-restricted pp65-CTL was lower than Tax-CTL at any peptide concentration. Furthermore, no specific IFN-γ production by HLA-A*24:02 pp65-CTL could be detected at all at peptide concentrations of 0.01–1 pM. In general in the literature, peptide concentrations of other viral or tumor antigen epitopes that the corresponding specific CTL recognize and respond to are in the range 1 nM–10 μM, although this varies according to the antigen.[28–32] Collectively, the results presented here indicate that the TCR avidities of these Tax-CTL can be considered to be extremely high.

Expression of human T-lymphotropic virus type 1 Tax in adult T-cell leukemia/lymphoma cells. Given the high TCR avidity of Tax-CTL, we next analyzed whether these CTL could recognize, respond to and kill ATL cells. To this end, Tax expression in ATL cell lines, HTLV-1-immortalized lines, K562 and short-term cultured primary ATL cells was assessed (Fig. 3). Tax expression was detected both by flow cytometry and RT-PCR in TL-Su, TCL-Kan, HUT102, MT-2 and MT-4, but not in K562, MT-1 or TL-Om1 by either technique. No Tax protein was seen in ATN-1 or in short-term cultured primary ATL cells from patients 7, 8 and 14, although *Tax* mRNA was present at levels 1/10–1/100th of those in TL-Su.

Tax-specific CTL responses against autologous adult T-cell leukemia/lymphoma cells. PBMC from patient 7 were stimulated with HLA-A*24:02 restricted Tax301–309 peptide, and the resulting CTL were expanded (Fig. 4A, upper-left panel).

Table 1. Tax-specific CTL expansion in adult T-cell leukemia/lymphoma (ATL) patients

Patient number	Clinical subtype	ATL status at blood sampling	Total cells (number)		Tax tetramer + cells/ lymphocytes (%)		Tax tetramer + cells (number)		Expansion rate†
			Day 0	Day 14	Day 0	Day 14	Day 0	Day 14	
Patient 1	Acute	Complete remission	4.5×10^6	9.5×10^6	0.01	4.51	4.5×10^2	4.28×10^5	951.1
Patient 2	Acute	Complete remission	3.0×10^6	2.8×10^6	<0.01	10.02	$<3.0 \times 10^2$	2.81×10^5	936.7
Patient 3	Chronic	Complete remission	8.6×10^6	1.5×10^7	0.02	9.02	1.72×10^3	1.35×10^6	784.9
Patient 4	Lymphoma	Complete remission	7.5×10^6	1.1×10^7	0.06	10.92	4.5×10^3	1.02×10^6	226.7
Patient 5	Acute	Complete remission	3.0×10^6	1.0×10^7	0.03	0.15	9.0×10^2	1.50×10^4	16.7
Patient 6	Lymphoma	Complete remission	4.3×10^6	3.5×10^6	<0.01	0.62	$<4.3 \times 10^2$	2.17×10^4	>50.5
Patient 7	Chronic	Watchful waiting	2×10^7	1.0×10^8	1.32	12.50	2.64×10^5	1.25×10^7	47.3
Patient 8	Chronic	Watchful waiting	6.5×10^6	9.2×10^6	0.01	7.05	6.5×10^2	6.49×10^5	998.5
Patient 8′‡	Acute	Before treatment	5.26×10^6	5.5×10^6	0.02	0.02	1.05×10^4	1.10×10^4	1.05
Patient 8″‡	Acute	Partial remission	3.5×10^6	6.8×10^6	0.06	26.36	2.1×10^3	1.79×10^6	852.4
Patient 9	Smoldering	Under systemic phototherapy for skin	3.0×10^6	5.8×10^6	0.02	28.78	6.0×10^2	1.67×10^6	2783.3
Patient 10	Lymphoma	Initially diagnosed	7.3×10^6	1.2×10^7	<0.01	0.28	$<7.3 \times 10^2$	3.36×10^4	>46.0
Patient 11	Acute	Initially diagnosed	4.3×10^6	4.1×10^6	<0.01	0.14	$<4.3 \times 10^2$	5.74×10^3	>13.3
Patient 12	Acute	Initially diagnosed	5.2×10^6	ND	ND	ND	ND	ND	ND
Patient 13	Acute	Initially diagnosed	1.0×10^7	ND	ND	ND	ND	ND	ND
Patient 14	Acute	Diagnosed as relapse with acute type phenotype	6.0×10^6	7.0×10^6	0.01	0.03	6.0×10^2	2.10×10^3	3.5
Patient 14 (CD4-subset)§			6.0×10^6	2.6×10^6	0.01	3.79	6.0×10^2	9.90×10^4	165.0

†Cell numbers of Tax tetramer + cells on day 14 was divided by that of day 0. ‡Patient 8 progressed from chronic to acute subtypes, and then he received allogeneic hematopoietic stem cell transplantation. §CD4+ cells were depleted on day 4. ATL, adult T-cell leukemia/lymphoma; CTL, cytotoxic T lymphocytes; HTLV-1, human T-lymphotropic virus type-1; ND, not detected.

In this culture, HLA-A2-restricted Tax11–19 specific CTL were also expanded (Fig. 4A, middle-left panel), even though the Tax11–19 peptide was not used as a stimulator. We surmised that pre-existing Tax-CTL, including these HLA-A2 Tax11–19 CTL, were stimulated by the ATL cells constitutively expressing HLA-A2/Tax11–19 complexes, contained in the cultured PBMC. These expanded T-cells were co-cultured with ATL cell lines, HTLV-1-immortalized lines or autologous ATL cells, and their responses were evaluated by IFN-γ production. HLA-A*24:02/Tax301–309 tetramer-positive fractions of these expanded CD8-positive cells produced IFN-γ when co-cultured with autologous ATL cells or ATN-1 (Fig. 4A), even though the Tax expression was so low as to be undetectable by flow cytometry, and only detectable by RT-PCR (Fig. 3). These tetramer-positive cells also responded to TL-Su and MT-2, but did not respond to the other ATL cell lines, or HTLV-1-immortalized lines tested. This indicates that only target cells having both HLA-A*24:02 and Tax were recognized (Table 2 and Fig. 3). The HLA-A*24:02/Tax301–309 tetramer-negative fractions of these expanded CD8-positive cells also produced IFN-γ when stimulated with autologous ATL cells. This suggests that they recognize unidentified Tax-derived epitopes, or antigens derived from HTLV-1 components other than Tax, or ATL-related tumor antigens not of viral origin. Finally, the HLA-A*02:01/Tax11–19 tetramer-positive fractions within these expanded CD8-positive cells were also found to produce IFN-γ on challenge with autologous ATL cells and TCL-Kan, but not the other ATL cell lines or HTLV-1-immortalized lines. This indicates that HLA-A2 and Tax expression were both required for recognition. HLA-A*02:01/Tax11–19 tetramer-negative cells also produced IFN-γ when stimulated by TCL-Kan. Because both patient 7 and TCL-Kan share HLA-B*46:01 and HLA-C*01:02 (Table 2), the tetramer-negative cells might be recognizing unidentified Tax-derived epitopes, other HTLV-1 antigens or ATL tumor antigens-derived epitopes presented on a different shared MHC allele. These effector cells did not respond to K562 by IFN-γ production, showing that they had no NK activity.

Next, PBMC from patient 8 at chronic stage were investigated in a similar manner, stimulated with Tax11–19 peptide (Fig. 4B, upper-left panel). HLA-A*02:01/Tax11–19 tetramer-positive cells in these expanded CD8-positive cells also produced IFN-γ (Fig. 4B) when stimulated with Tax RT-PCR-positive but flow cytometry-negative autologous ATL cells

Table 2. Human leukocyte antigen (HLA) information

	HLA-A		HLA-B		HLA-C	
TL-Su	*11:01	*24:02	*15:01	*40:02	*03:04	*04:01
TCL-Kan	*02:06	*02:07	*46:01	*56:01	*01:02	*07:02
K562						
HUT102	*30:02	*66:02				
ATN-1	*11:01	*24:02	*54:01	*67:01	*01:02	*07:02
MT-1	*11:01	*26:01	*39:01	*40:02	*03:04	*07:02
MT-2	*24:02	*24:02	*40:02	*51:01	*03:03	*14:02
MT-4	*11:01	*31:01	*39:02	*67:01	*07:02	*07:02
TL-Om1	*02:01	*02:01	*52:01	*52:01	*12:02	*12:02
Patient 1	*02:01	*02:01	*15:01	*40:02	*03:04	*07:02
Patient 3	*02:01	*31:01				
Patient 4	*24:02	*26:01				
Patient 5	*02:06	*24:02				
Patient 6	*02:06	*31:01				
Patient 7	*02:07	*24:02	*46:01	*52:01	*01:02	*12:02
Patient 8	*02:01	*02:06	*35:01	*55:02	*01:02	*03:03
Patient 9	*02:01	*31:01				
Patient 10	*11:01	*24:02				
Patient 11	*11:01	*24:02				
Patient 12	*02:06	*24:02				
Patient 13	*02:03	*31:01				
Patient 14	*24:02	*31:01	*07:02	*40:01	*03:04	*07:02

doi: 10.1111/j.1349-7006.2012.02371.x

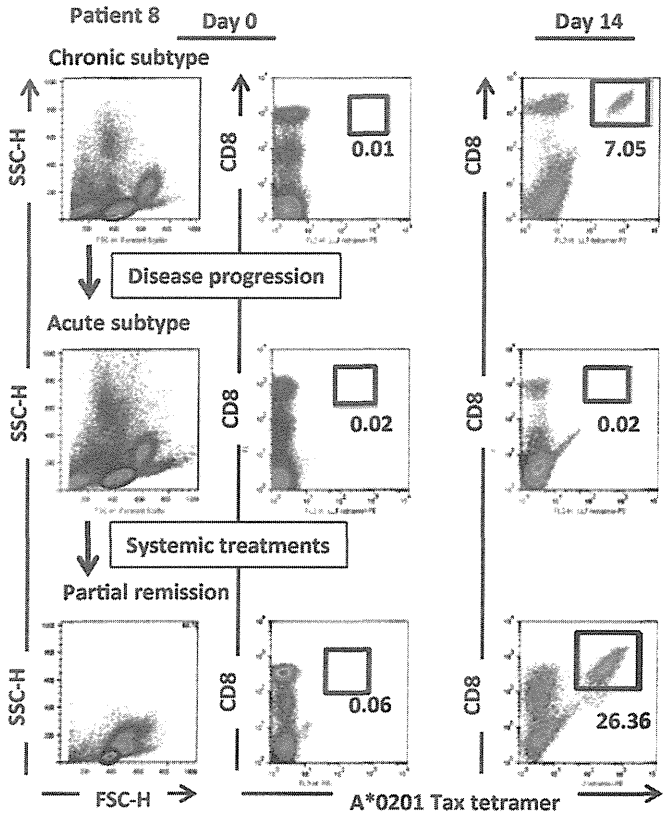

Fig. 1. Expansion of Tax-specific CTL from PBMC of patient 8 at different clinical stages. Flow cytometric analyses of the expanded cells are presented. The lymphocyte population was determined by FSC-H and SSC-H levels (left panels) and the data are plotted to show CD8 and human leukocyte antigen (HLA)-A*02:01/Tax tetramer-positivity (right two panels). Both CD8 and HLA-A*02:01/Tax tetramer-positive cells are gated, and their percentages relative to the entire lymphocyte population are indicated in each panel. Patient 8 progressed from chronic to acute stage disease. His Tax-CTL could be efficiently expanded during the chronic phase (upper panels), but no longer after progression to acute stage (middle panels). Subsequently, he received allogeneic hematopoietic stem cell transplantation, and achieved partial remission. At this time, his Tax-CTL could be efficiently expanded from PBMC once more (lower panels).

(Fig. 3). These tetramer-positive cells responded to TCL-Kan but not to the other ATL cell lines or HTLV-1-immortalized lines. Thus, their recognition was also restricted by the expression of HLA-A2 and Tax (Table 2 and Fig. 3). HLA-A*02:01/Tax11–19 tetramer-negative fractions were also stimulated by autologous ATL cells, again suggesting recognition of unidentified epitopes. HLA-A*02:01/Tax11–19 tetramer-negative cells also produced IFN-γ when stimulated by TCL-Kan. Because patient 8 and TCL-Kan are both HLA-C*01:02-positive (Table 2), these effector cells might be recognizing unidentified epitopes presented on this shared MHC allele. Again, there was no IFN-γ production against K562.

We also repeated these experiments with PBMC from patient 14, and evaluated them in the same manner. In this case as well, the HLA-A*24:02/Tax301–309 tetramer-positive cells responded to autologous ATL cells and ATN-1 (Fig. 4C), again despite the very low level of Tax expression. They also responded to TL-Su, but not the other ATL cell lines or HTLV-1-immortalized lines, showing HLA-A*24:02 and Tax restriction (Table 2 and Fig. 3). Once more, the HLA-A*24:02/Tax301–309 tetramer-negative cells were also stimulated by autologous ATL cells, indicating recognition of unidentified epitopes presented on autologous MHC molecules. HLA-A*24:02/Tax301–309 tetramer-negative cells also produced IFN-γ when stimulated with TL-Su, which shares HLA-C*03:04 with patient 14 (Table 2). Again, no NK activity was detectable.

Lysis of autologous adult T-cell leukemia/lymphoma cells by Tax-specific CTL. Cells from patient 7 expanded by Tax301–309 peptide (Fig. 4A) killed TL-Su, MT-2, ATN-1 and autologous ATL cells in an E/T ratio-dependent manner, but did not lyse MT-1 or HUT102 (Fig. 5, left panel). Lysis depended on the presence of both HLA-A*24:02 and Tax (Table 2 and Fig. 3). Although as mentioned before, the level of Tax expression by these autologous ATL cells and ATN-1 was so low as to be detectable only by RT-PCR and not by flow cytometry, objective lysis of both cells was still observed. The patient 7 Tax-CTL expanded by Tax301–309 peptide stimulation also killed TCL-Kan. HLA-A2-restricted Tax11–19 CTL included in the effector subset presumably contributed to the lyses of TCL-Kan as well as autologous tumor cells (Fig. 4A, middle-left panel). Again, these expanded cells did not possess NK activity. The cells from patient 8 at chronic stage expanded by Tax11–19 peptide (Fig. 4B) killed TCL-Kan and autologous ATL cells, but not TL-Om1 (Fig. 5, middle panel) in an HLA-A2-restricted and Tax-restricted manner (Table 2 and Fig. 3). Again, Tax expression by the autologous ATL cells was extremely low, but the targets were, nonetheless, killed. As with the other patients, there was no NK activity present in the expanded cells.

Finally, cells from patient 14 stimulated by Tax301–309 peptide (Fig. 4C) killed TL-Su and autologous ATL cells, but not MT-1 (Fig. 5, right panel), restricted by HLA-A*24:02 and Tax (Table 2 and Fig. 3), again with no NK activity.

Tax expression in primary adult T-cell leukemia/lymphoma cells induced by short-term culture. It was previously reported that although Tax expression was not detectable in primary ATL cells by flow cytometry in most cases, short-term culture of such cells could induce Tax expression in nearly half of cases.[33] Tax expression and its regulation in primary ATL cells is currently not fully understood. We tested Tax expression of primary ATL cells from patients 7, 8, 13 and 14, as listed in Table 1, and 2 additional patients, 15 and 16 (both chronic type). Tax protein was not present in any primary uncultured ATL cells isolated with anti-human CD4 microbeads from patients' peripheral blood. In all cases, these cells were in a quiescent state, as determined by 7-AAD staining (Fig. 6A). Cells incorporating BrdU (S phase) and those having double DNA content (G2/M phase) first appeared on culture of the primary ATL cells for several days, indicating that they had begun to cycle. At the same time, Tax-expressing cells appeared in three of six cases (patients 7, 8 and 13) (Fig. 6B). These findings indicate that Tax expression was induced in primary ATL cells when they were actively cycling (i.e. cells not in G0 phase). Because most primary ATL cells in the peripheral blood are in a quiescent state (G0 phase), they express little or no Tax.

Tax expression in primary adult T-cell leukemia/lymphoma cell-bearing NOG mice. NOG mice bearing primary ATL cells were established using ATL cells of patients 7, 12 and 13, as previously described.[34] ATL mice from patient 7 presented with large intraperitoneal tumor masses, and tumor cells aggressively infiltrated into liver and spleen, but into the blood only to a lesser extent. Setting the *Tax/human CD4* mRNA level of TL-Su as unity, these values for blood cells, liver, spleen and tumor cell suspensions were 0.00195 ± 0.00065 (standard deviation), 0.023000 ± 0.00312, 0.00626 ± 0.00214 and 0.19533 ± 0.02185, respectively. Because there was little ATL cell infiltration into bone marrow, the *Tax/human CD4* mRNA value of bone marrow cells was under the limit of detection

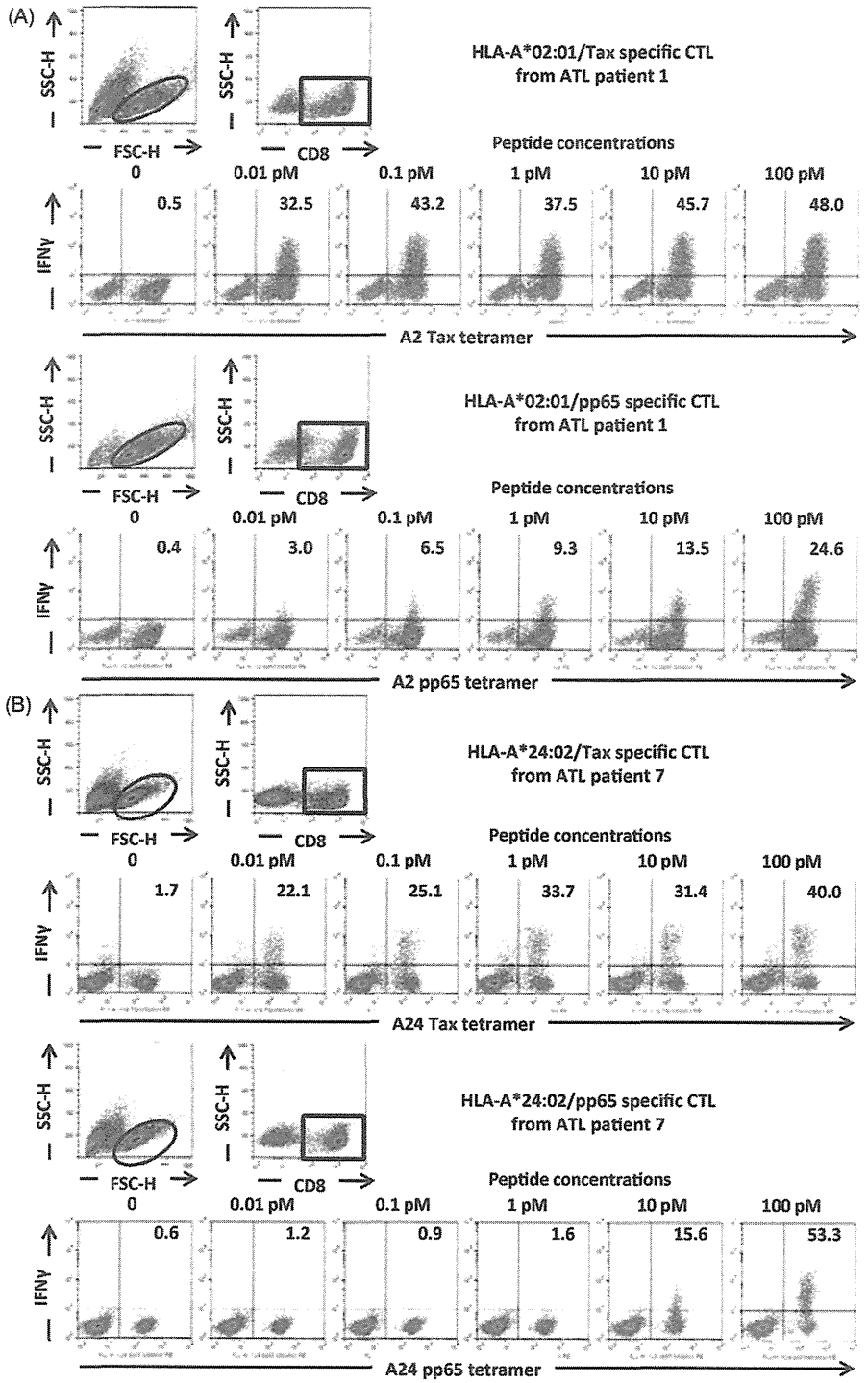

Fig. 2. T-cell receptor avidity of Tax-CTL for Tax epitope peptides. (A) PBMC from adult T-cell leukemia/lymphoma (ATL) patient 1 were stimulated by Tax11–19 peptide, and the expanded cells were then cultured with serial concentration of the cognate peptide. Flow cytometric analyses of those cells are presented. The lymphocyte population was identified by FSC-H and SSC-H levels, and CD8-positive cells gated. These were then plotted according to human leukocyte antigen (HLA)-A*02:01/Tax tetramer-positivity and interferon gamma (IFN-γ) production. The percentages of IFN-γ-producing cells relative to the entire population of HLA-A*02:01/Tax-positive cells are indicated in each panel (upper panels). PBMC from ATL patient 1 were also stimulated by CMV-pp65 495–503 peptide, and then restimulated with the cognate peptide, and flow cytometric analyses of those cells are presented in the same manner as above. The percentages IFN-γ-producing cells relative to the entire population of HLA-A*02:01/CMV-pp65-positive cells are indicated in each panel (lower panels) (B) PBMC from ATL patient 7 were stimulated with Tax301–309 peptide, and then restimulated as above: HLA-A*24:02/Tax301–309 tetramer positivity and IFN-γ production (upper panels). PBMC from ATL patient 7 stimulated with CMV-pp65 495–503 peptide, and treated as above. Each result represents three independent experiments.

doi: 10.1111/j.1349-7006.2012.02371.x

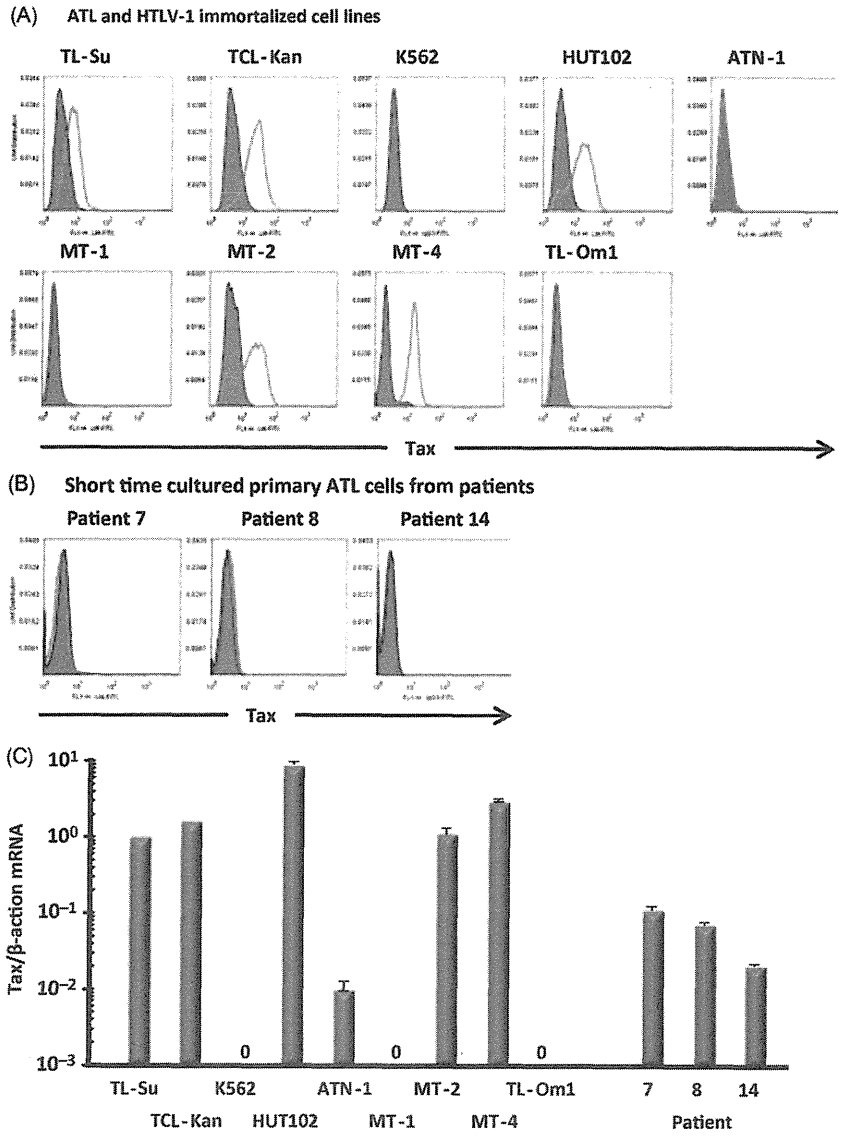

Fig. 3. Expression of human T-lymphotropic virus type 1 (HTLV-1) Tax in adult T-cell leukemia/lymphoma (ATL) cells. (A) Tax expression in ATL cell lines, HTLV-1-immortalized lines and K562 were analyzed by flow cytometry. The cells lines were stained with anti-Tax mAb (blank histograms) or isotype control mAb (filled histograms). (B) Tax expression in short-term cultured ATL cells from patients analyzed by flow cytometry. (C) *Tax* expression in the cell lines and short-term cultured ATL cells from patients analyzed by quantitative RT-PCR by dividing the *Tax* expression level by *β-actin*, resulting in a *Tax/β-actin* mRNA ratio with the expression level in TL-Su set at unity. Columns, mean of triplicate experiments; bars, standard deviation.

(Fig. 7A). *Tax* expression in ATL cells from tumor masses was almost 100-fold higher than in the blood.

ATL mice from patient 12 presented with marked hepatosplenomegaly, but few tumor cells in the blood. *Tax/human CD4* mRNA values of blood cells, liver, and spleen cell suspensions were 0.01337 ± 0.00083, 0.05277 ± 0.00805 and 0.08323 ± 0.00080, respectively. Again, no *Tax/human CD4* mRNA could be detected in bone marrow cells (Fig. 7B).

Adult T-cell leukemia/lymphoma mice from patient 13 also presented with marked hepatosplenomegaly, but also with tumor infiltration into blood and bone marrow. *Tax/human CD4* mRNA values of blood cells, liver, spleen cell suspensions and bone marrow cells were 0.01013 ± 0.00102, 0.12742 ± 0.01524, 0.15411 ± 0.01612 and 0.28881 ± 0.07319, respectively (Fig. 7C).

These observations are consistent with other results from the present study that Tax expression is observed predominantly in actively cycling ATL cells, whereas most primary ATL cells in the peripheral blood are in a quiescent state. Thus, only ATL cells present at the site of active cell proliferation, such as in the tumor masses, liver or spleen, strongly express Tax, but this factor is minimally expressed by the tumor cells in a quiescent state, such as in the blood.

Discussion

The significant findings in the present study are as follows. The efficiency of *in vitro* Tax-CTL expansion was dependent on the stage of disease development following HTLV-1 infection. HTLV-1 Tax-CTL expanded *in vitro* could recognize HLA/Tax-peptide complexes on autologous ATL cells, the Tax expression of which was so low as to be detectable only by RT-PCR and not by flow cytometry. Tax recognition resulted in the production of IFN-γ and killing of the target cells. In an assay of TCR avidity, both HLA-A*02:01-restricted and HLA-A*24:02-restricted Tax-CTL responded to as little as 0.01 pM of the epitope peptide, a concentration much lower than required for recognition of any other viral or tumor antigens. This documents the extremely high TCR avidity of Tax-CTL, which is presumably one of the reasons why these CTL could recognize and kill the autologous ATL cells, despite their very low Tax expression. To the best of our knowledge, this is the first report of Tax-specific CTL from ATL patients specifically recognizing and killing autologous tumor cells that express the Tax antigen. Earlier studies examined the responses of CD8 cells against autologous cells from ATL, HTLV-1-associated myelopathy/tropical spastic paraparesis patients or HTLV-1